

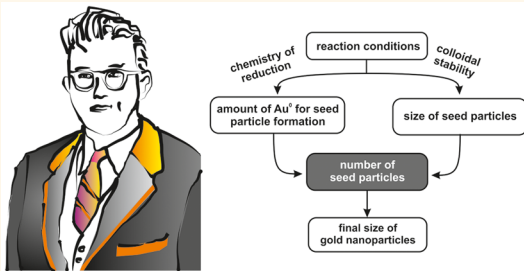


Turkevich in New Robes: Key Questions Answered for the Most Common Gold Nanoparticle Synthesis

Maria Wuithschick,[†] Alexander Birnbaum,[†] Steffen Witte,[†] Michael Sztucki,[‡] Ulla Vainio,[§] Nicola Pinna,[†] Klaus Rademann,[†] Franziska Emmerling,^{||} Ralph Krahnert,[⊥] and Jörg Polte^{*,†}

[†]Department of Chemistry, Humboldt-Universität zu Berlin, Brook-Taylor-Straße 2, 12489 Berlin, Germany, [‡]ESRF - The European Synchrotron, 71 Avenue des Martyrs, 38043 Grenoble, France, [§]Deutsches Elektronen-Synchrotron, Notkestraße 85, 22607 Hamburg, Germany, ^{||}BAM Federal Institute of Materials Research and Testing, Richard-Willstätter-Straße 11, 12489 Berlin, Germany, and [⊥]Technische Universität Berlin, Straße des 17. Juni 124, 10623 Berlin, Germany

ABSTRACT This contribution provides a comprehensive mechanistic picture of the gold nanoparticle synthesis by citrate reduction of HAuCl₄, known as Turkevich method, by addressing five key questions. The synthesis leads to monodisperse final particles as a result of a seed-mediated growth mechanism. In the initial phase of the synthesis, seed particles are formed onto which the residual gold is distributed during the course of reaction. It is shown that this mechanism is a fortunate coincidence created by a favorable interplay of several chemical and physicochemical processes which initiate but also terminate the formation of seed particles and prevent the formation of further particles at later stages of reaction. Since no further particles are formed after seed particle formation, the number of seeds defines the final total particle number and therefore the final size. The gained understanding allows illustrating the influence of reaction conditions on the growth process and thus the final size distribution.



KEYWORDS: Turkevich · gold nanoparticles · growth mechanism · size control · tetrachloroauric acid · SAXS

The applications of gold nanoparticles (AuNP) are diverse due to their unique catalytic, biological and optical properties.¹ The most commonly used synthesis of colloidal gold in aqueous solution is the reduction of tetrachloroauric acid (HAuCl₄) with trisodium citrate (Na₃Ct).^{2–5} In the past decade, the citrate method has increasingly been referred to as “Turkevich synthesis”, named after John Turkevich who described the reaction in 1951.⁶ Although the work of Turkevich and his co-workers is certainly a landmark for the synthesis of AuNP, the naming of the synthesis is historically not quite correct if intended to honor the discoverers. Turkevich *et al.* referred to the textbook *Experiments in Colloid Chemistry* by Ernst A. Hauser and J. Edward Lynn, already published in 1940, who reported the formation of gold colloids upon reacting HAuCl₄ and Na₃Ct.⁷ Until today, the original synthesis protocol was modified numerous times allowing the fabrication of AuNP in a wide range of sizes.^{5,6,8–10}

Most syntheses of colloidal nanoparticle solutions are poorly understood in terms of

the growth mechanism. In general, this is attributed to the fact that appropriate data on the size evolution during particle formation is difficult to obtain.¹¹ In the case of the Turkevich method, a surprisingly large number of contributions deal with the particle growth process or the molecular reduction mechanism, which emphasizes the general importance of this synthetic procedure. However, the multitude of publications does not lead to a comprehensive understanding of the growth governing processes since the published interpretations are manifold and not consistent. Turkevich and co-workers gave the very first description of the growth process. They investigated the synthesis astonishingly detailed using a wide range of analytical methods (slit-ultramicroscopy, nephelometry and electron microscopy).^{6,12} Turkevich *et al.* applied a nucleation and growth model similar to the theory shown by LaMer and Kenyon for the formation of colloidal sulfur,¹³ although it was pointed out that the observed temperature dependence of the nucleation rate

* Address correspondence to joerg.polte@hu-berlin.de.

Received for review March 12, 2015 and accepted July 6, 2015.

Published online July 06, 2015
10.1021/acsnano.5b01579

was difficult to understand from that perspective. An “organizer model” was established attributing a decisive role to the formation of large macromolecules of gold ions and reducing agent with nucleation events being induced by dicarboxy acetone (DCA), an oxidation product of Na₃Ct formed during the synthesis. The nucleation-diffusional growth mechanism was generally accepted for many decades, also in the highly recognized work of Frens.⁸

In contrast, a contribution published only a few years after the work of Turkevich *et al.* remained almost unnoticed despite its excellent scientific quality. Kazuyoshi Takiyama investigated the citrate method using electron microscopy (EM) and UV-vis spectroscopy. From EM in combination with the spray method, the AuNP concentration could be estimated during the course of reaction.¹⁴ The results revealed that the number of particles is determined in the very initial phase of the synthesis and remains constant during the later course of reaction.

Later scientific work on the growth mechanism was often focused on an observation which is made shortly after mixing the reactants. The synthesis solution appears gray-bluish before turning into purple and the well-known ruby red color which is characteristic for spherical AuNP in the size range of $r \sim 5\text{--}15\text{ nm}$.¹⁵ In 1994, Chow and Zukoski attributed the gray-blue color during the initial stage of the synthesis to the reversible aggregation of primary particles.⁹ This hypothesis has been supported and refined by several other groups. Pei *et al.* reported the formation of 2D gold nanowires networks for low citrate concentrations.¹⁶ Rodríguez-González and co-workers observed a sudden shift of the redox potential from +0.75 V *versus* Ag/AgCl to +0.1 V at the end of the reaction, which they correlated to the peptization of aggregates to form the final monodisperse particles.¹⁷ Pong *et al.* proposed the formation of linear assemblies from clusters, adsorption of more Au atoms, defragmentation and aging *via* Ostwald ripening.¹⁸ Ji and co-workers deduced a pH dependent growth mechanism which also comprises the formation of aggregates and intraparticle ripening for pH values below 6.5 (refers to pH after mixing the reactants).¹⁹ Although not consistent with their small-angle X-ray scattering (SAXS) experiments, Mikhlin *et al.* proposed a growth mechanism involving the formation of dense liquid domains enriched with Au clusters and complexes followed by the formation of AuNP aggregates, which separate during the course of the reaction.²⁰ The formation of wire-like aggregates as an intermediate step was also reported by Zhao and co-workers.²¹ All these mechanisms, which comprise the formation of any kind of aggregate intermediates during the Turkevich synthesis, were derived mainly from UV-vis and TEM data. In this contribution, it will be shown that the origin of the gray-bluish color during the initial phase of the

synthesis was misinterpreted: large Au aggregates are not formed at any time of the Turkevich synthesis.

Simultaneously to the establishment of the different nanowire theories, the nucleation-diffusional growth model proposed by Turkevich *et al.* still remained widely accepted.^{2,3,22} Kumar *et al.* even developed a quantitative model based on this growth mechanism including also Turkevich's organizer model.²³ Recently, Georgiev and co-workers suggested a Finke-Watzky growth mechanism,²⁴ which consists of a slow, continuous nucleation and a fast autocatalytic growth.²⁵ Their assumption is based on fitting an exponential rate equation to kinetic data (derived from *ex situ* AFM measurements) which shows a sigmoidal-curve shape.

Polte *et al.* developed a synchrotron setup which allows simultaneous SAXS and X-ray absorption near edge spectroscopy (XANES) measurements for liquid samples.^{26,27} With this setup, time-resolved data on particle size distribution, relative particle concentration and reduction of Au³⁺ to Au⁰ could be obtained which allows to monitor the particle growth *in situ*. The deduced growth mechanism is explained in detail later in this contribution.

In 2010, a molecular mechanism for the reduction of Au³⁺ during the Turkevich synthesis was proposed.² Modeling of this reduction mechanism under different pH conditions using DFT calculations contributed to a better description of the underlying Au³⁺ reduction process.²⁸ However, the results remained unrelated to the particle growth mechanism though the growth obviously depends on the supply of monomers and thus on the reduction process. In general, we are yet far from understanding the influences of synthesis parameters on the growth process and thus the final size. Only the combination of the chemical reduction process and the physicochemical particle growth can deliver a full and comprehensive picture of the Turkevich synthesis.

In this contribution, essential key questions of the Turkevich synthesis are addressed, which lead to a profound picture of the Turkevich method's growth mechanism:

1. What is the general growth mechanism of the Turkevich synthesis?
2. When is the final particle size determined?
3. What determines the final particle size?
4. How do synthesis parameters influence the particle growth and therefore the final size?
5. Why does the citrate reduction of silver nitrate (AgNO₃) not result in monodisperse and uniform particles as for HAuCl₄?

RESULTS AND DISCUSSION

Question #1: What Is the General Growth Mechanism of the Turkevich Synthesis? As mentioned in the introduction, the number of proposed growth mechanisms is almost the same as the number of publications on the topic

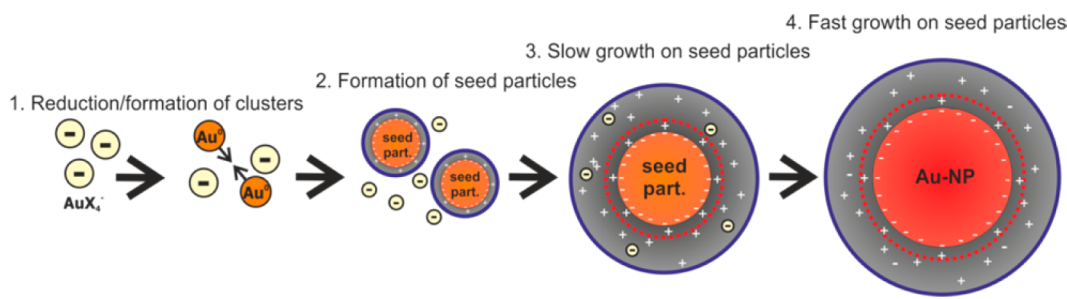


Figure 1. General growth mechanism of the Turkevich synthesis as deduced by Polte.³² Herein, this growth mechanism is shown to be valid for a wide range of parameter variations.

itself. Therefore, the starting point for a comprehensive study on the Turkevich synthesis needs to be a discussion of the general growth mechanism.

Most of the deduced Turkevich mechanisms are derived from analytical methods which (i) might not reflect the properties of the colloidal solution (*ex situ* methods, *e.g.* electron microscopy), (ii) cannot deliver decisive information on the particle concentration (*e.g.*, UV-vis spectroscopy), or (iii) cannot be applied in a sufficient time-resolution (*e.g.* *in situ* AFM²⁰). SAXS was shown to be a versatile tool for the investigation of nanoparticle growth mechanisms since it delivers *in situ* information on the particle size distribution and the relative particle concentration.^{29–31} Combined with a free liquid jet, the method offers the benefits of a container-free measurement (avoiding contamination problems) and minimized inducing effects of the incident X-ray beam. If the setup is applied at a synchrotron light source, the time-resolution can be in the range of milliseconds. Coupled with XANES, simultaneous tracking of the chemical reduction becomes available. Therefore, time-resolved SAXS/XANES measurements deliver the decisive information necessary to deduce a comprehensive growth mechanism of the Turkevich synthesis.

A schematic, which can be found in Figure 1, illustrates the mechanism deduced from SAXS/XANES measurements by Polte *et al.*^{26,27} which was refined recently.³² The mechanism comprises four steps. The first step is a partial reduction of the gold precursor and the formation of small clusters from the Au monomers. In a second step, these cluster form seed particles with radii >1.5 nm. The remaining gold ions are attracted and attached in the electronic double layer (EDL) of the seed particles as co-ions. The third and fourth step comprise the reduction of the ionic gold (first slowly, then fast) whereby the generated gold monomers grow exclusively on top of the seed particles' surfaces until the precursor is fully consumed. Therefore, no further particles are formed during the last two steps. It should be mentioned that as early as 1958, Takiyama also recognized that the number of particles remains constant after a short initial phase. Nevertheless, the time resolution of his applied experimental procedure was very limited.¹⁴ Although Takiyama

deduced a crucial point of the growth mechanism, his work remained widely unrecognized.

The described mechanism can be referred to as seed-mediated growth mechanism. It can be distinguished clearly from a so-called nucleation–growth mechanism. The latter is based on the formation of “nuclei”, a term which refers to the first thermodynamically stable clusters which in general consist of only few atoms. In contrast, the herein described growth mechanism is based on the formation of seed particles, which already have stable sizes and consist of some hundred atoms (for example, a AuNP with $r = 1.5$ nm consist of ~ 840 atoms).

As mentioned above, several publications claim the formation and subsequent fragmentation of large gold aggregates in the beginning of the Turkevich synthesis.^{9,16–21} This assumption is based on the shift of the plasmon band maximum from 530 nm to approximately 520 nm during the early stage of the synthesis (corresponding to a color change from bluish-purple to red), time-resolved DLS measurements and *ex situ* TEM images which show large networks of particles. To disprove this hypothesis, ultrasmall angle X-ray scattering (USAXS) measurements at different reaction times were made at the DORIS III synchrotron light source using a flow-through capillary. USAXS allows to detect AuNP aggregates since the determination of large objects ($r > 25$ nm) demands the measurement at very small angles (corresponds to low \mathbf{q} values, with scattering vector magnitude defined as $\mathbf{q} = (4\pi/\lambda)\sin \theta$). Figure 2 shows selected scattering curves and corresponding fits for a Turkevich synthesis carried out under same conditions as described in literature²⁶ ($T = 75$ °C, final concentrations $[\text{HAuCl}_4] = 0.25$ mM, $[\text{Na}_3\text{Ct}] = 2.5$ mM, mixing of equal reactant volumes). Even at the minimal accessible angle, which corresponds to $\mathbf{q} = 0.04$ nm⁻¹, no significant scattering signal is detected throughout the synthesis. This confirms that large structures are not formed at any time of the Turkevich synthesis. The bluish color of the reaction solution at the early stages is most likely caused by the attachment of gold ions in the EDL of the seed particles and a change of their electronic properties.³² Charging effects are known to influence the optical properties of AuNP significantly.^{15,33}

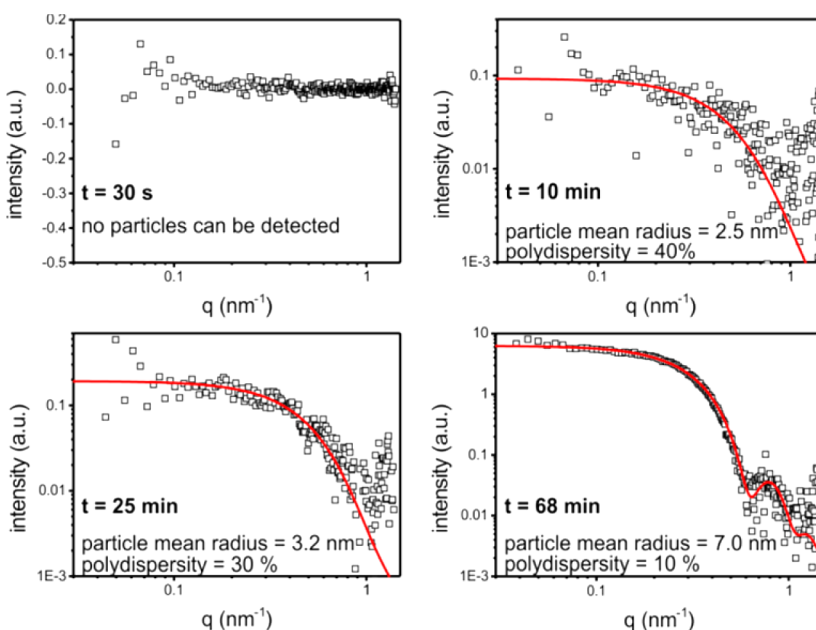


Figure 2. Selected scattering curves and corresponding mathematical fits of time-resolved USAXS measurements. The reaction conditions were in accordance to a previous publication²⁶ ($T = 75\text{ }^\circ\text{C}$, $[\text{HAuCl}_4] = 0.25\text{ mM}$, $[\text{Na}_3\text{Ct}] = 2.5\text{ mM}$, mixing of equal reactant volumes).

Aggregates, which were observed in TEM images of samples taken during early stages of the synthesis, are most likely artifacts formed during the sample preparation process (drying) and do not represent the actual properties of the colloidal solution. A detailed discussion on the existence or nonexistence of aggregates can be found in Supporting Information SI-1.

The proposed growth mechanism was derived from investigations using three different sets of reaction conditions (75 and $85\text{ }^\circ\text{C}$, $[\text{HAuCl}_4] = 0.25\text{ mM}$, $[\text{Na}_3\text{Ct}] = 2.5\text{ mM}$ and $75\text{ }^\circ\text{C}$, $[\text{HAuCl}_4] = 0.375\text{ mM}$, $[\text{Na}_3\text{Ct}] = 2.5\text{ mM}$, both mixing of equal reactant volumes).²⁵ To investigate the general validity of the deduced growth mechanism, another SAXS study with various sets of parameters including a variation of reactant concentrations, the way of mixing the reactants and temperature was carried out at the ESRF synchrotron light source. The results are shown in the Supporting Information (see SI-2). For all investigated parameter combinations, the different growth steps are observed. Only the duration of each particular step and the corresponding mean particle radii depend on the reaction conditions. The influence of reaction parameters on the growth process will be discussed in detail later in this contribution. From the parameter study, it can be concluded that the deduced growth mechanism is valid for a wide range of reaction conditions, at least for sets of parameters commonly used in Turkevich synthesis protocols.

Summary #1. The Turkevich synthesis is characterized by a seed-mediated growth mechanism. Stable seed particles with sizes of $r > 1.5\text{ nm}$ are formed in the beginning of the synthesis. Remaining gold ions are

attached and reduced in the EDL of the seed particles and grow exclusively onto the existing particles. Further particles are not formed. Therefore, the total number of particles at the end of the synthesis corresponds to the number of seed particles and is determined already in the beginning of the synthesis. The formation of large aggregates ("nanowires") during the course of the reaction can be excluded.

Question #2: When Is the Final Particle Size Determined?

According to the growth mechanism of the Turkevich synthesis, the final number of particles corresponds to the number of seed particles formed in step 2. The number of particles determines the final size because it defines to how many particles the total amount of gold (defined by initial HAuCl_4 concentration) is distributed. Therefore, the final particle size is already determined by the seed particle formation. Accordingly, step 2 of the growth mechanism is investigated in this section.

The end of step 2 corresponds to the point at which the relative number of particles remains constant. A direct determination of the according reaction time is difficult. The relative particle number can be derived from SAXS experiments, but a sufficient signal-to-noise ratio is required. In the beginning of the Turkevich synthesis (*i.e.*, during the seed formation step), the solution contains too few particles for a precise analysis of the particle concentration with SAXS. Nevertheless, the point at which the formation of seed particles is finished (end of step 2) can be determined using an indirect approach as illustrated in Figure 3a. A Turkevich synthesis is carried out under reflux. Aliquots are extracted from the batch at different reaction times and immediately cooled down to room temperature.

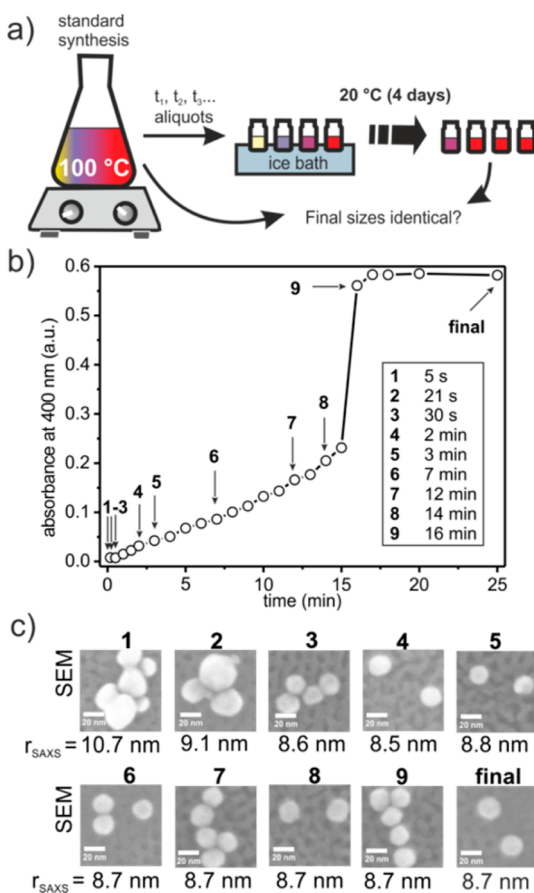


Figure 3. (a) Sketch of the quenching experiment to investigate at which reaction time the final size is determined; (b) UV-vis monitoring of absorbance at 400 nm versus time, corresponds to reduction progress; (c) representative SEM images and results of SAXS measurements after Au^{3+} reduction was completed at 20 °C (polydispersity of samples 1 and 2 = 30%, polydispersity of samples 3 to final = 10%).

The aliquots are kept at 20 °C for 4 days during which the entire amount of remaining gold slowly grows onto the preformed seed particles. For colloidal gold, the absorbance at 400 nm has been shown to be a good measure for the total amount of atomic gold.¹⁵ Therefore, the full precursor reduction of the aliquots can be checked by comparing their absorbance at 400 nm to the absorbance of the standard synthesis. The completed colloidal solutions (after 4 days) are investigated with electron microscopy and SAXS and compared to the particles of the standard batch. As evident from the growth mechanism, the total number of particles in the final colloidal solutions should be the same if an aliquot is taken after the seed formation (*i.e.*, after step 2). As a result, the final particle sizes should be identical. If an aliquot is taken before the end of the seed particle formation, step 2 will be disturbed and the number of seed particles of the aliquot would be different from the standard batch. The remaining amount of gold is distributed to more or less particles. As a result, the final particle size of the aliquot is either smaller or larger

compared to the standard batch. Therefore, the first reaction time at which the final size of an aliquot matches the size of the final standard solution is the point at the seed formation was completed. The described experiment (following denoted as quenching experiment) was carried out for a typical Turkevich synthesis. Over the last six decades, a variety of experimental protocols have been described. In this publication, the standard synthesis refers to the following procedure: 199 mL of a 0.25 mM HAuCl_4 solution are refluxed for 15 min. One milliliter of a 500 mM freshly prepared Na_3Ct solution is added quickly (final concentration $[\text{Na}_3\text{Ct}] = 2.5$ mM). The solution is refluxed until ruby red. For the quenching experiment, 9 aliquots were taken in the as-described procedure. In addition, the reduction progress was monitored during the course of the synthesis using UV-vis spectroscopy (monitoring the 400 nm absorbance). Figure 3b shows the absorbance at 400 nm *versus* time during the performed standard Turkevich synthesis and displays the reaction times at which aliquots were taken from the batch mix. Figure 3c displays the final mean particle radius of the aliquots and the final standard solution as determined with SAXS together with exemplarily SEM images. The final particle sizes determined with SAXS are in accordance to the sizes determined with SEM. In addition, selected aliquots were investigated with TEM (see Supporting Information SI-3). The mean particle radius of the final standard solution was 8.7 nm (polydispersity 10%). Aliquots 1 and 2 had final mean radii of 10.7 and 9.1 nm (both with high polydispersity of 30%), respectively. Aliquot 3, which corresponds to a reaction time of 30 s and a reduction progress of approximately 1.3% (determined from the absorbance at 400 nm), as well as the other aliquots showed almost the same mean particle radius as the final standard solution (between 8.5 and 8.8 nm, polydispersity 10%). This means aliquot 3 marks the end of the seed particle formation in the standard synthesis batch. Furthermore, the results support the deduced growth mechanism (see Figure 1) since they prove that the kinetics of the reduction process (some minutes at 100 °C, some days at 20 °C) are irrelevant with respect to the final size from a certain point of the synthesis. Steps 1 and 2 of the growth mechanism determine the final size, while the exact kinetics and reduction mechanism of step 3 and 4 have no influence.

Summary #2. The final size is determined at the end of the seed particle formation (step 2). For the standard synthesis with a total reaction time of approximately 17 min, the formation of seed particles proceeds approximately within the first 30 s at which approximately 1–2% of the gold precursor is reduced. Consequently, the final particle size is already determined within a very short time upon mixing the reactants. The kinetics of the following growth steps are irrelevant for the final particle size.

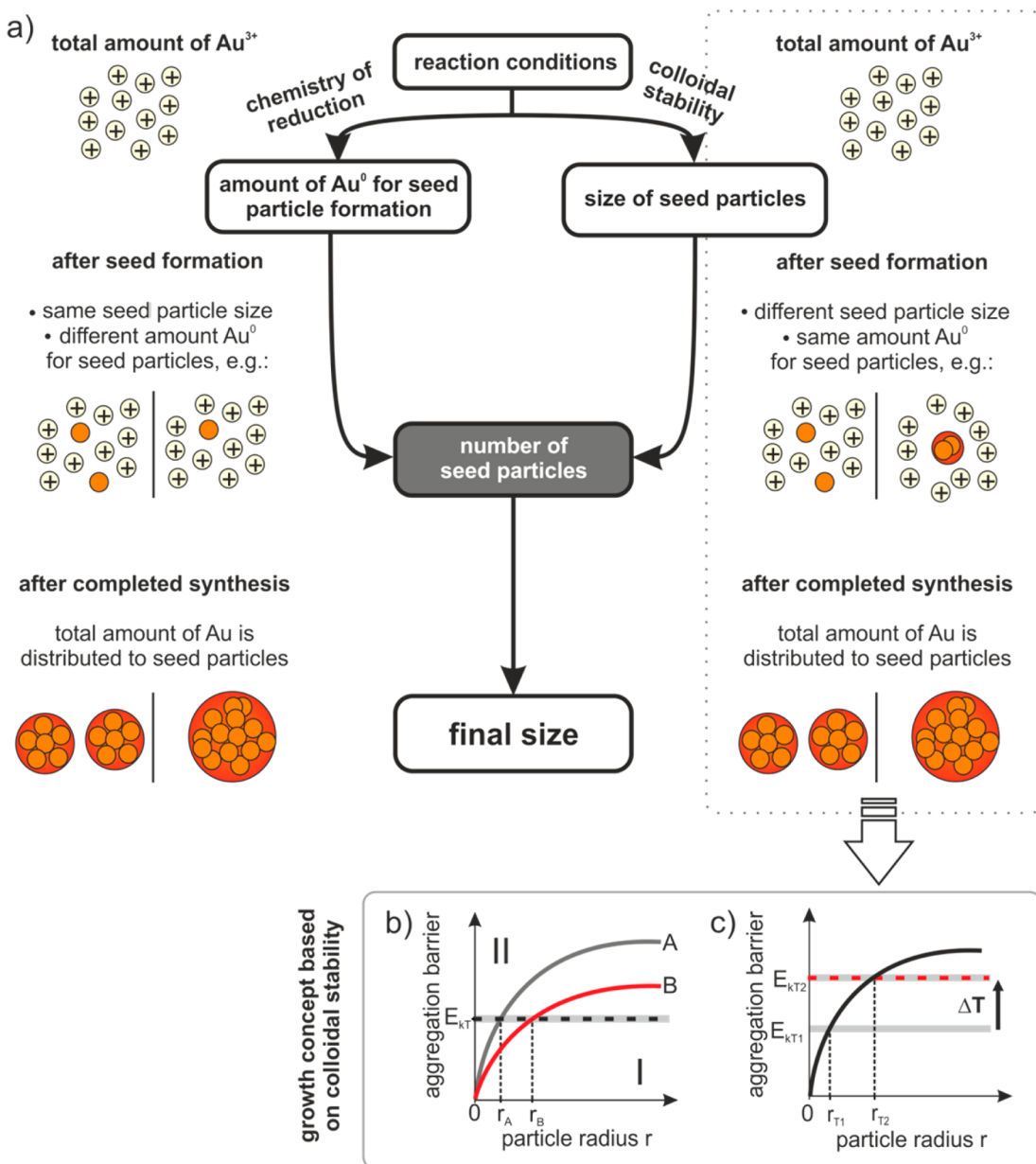


Figure 4. (a) Sketch to illustrate what determines the final particle size of the Turkevich synthesis. The final size depends on the total number of particles which corresponds to the number of seed particles. It is determined by the amount of Au monomers available for seed particle formation (left side) and the seed particle size (right side). Two examples for different amounts of Au monomers and different seed particle size, respectively, depict their influence on the final particle size. (b,c) Illustration of colloidal stability concept to describe reaction parameter influences on the size of NP. In this contribution, the concept is used to illustrate the influence of parameters on the size of seed particles. (b) Schematics of aggregation barrier versus particle radius for two different systems. E_{KT} corresponds to the available thermal energy. In area I, particle growth is initiated. In area II, stable colloids are obtained. (c) Schematics of influence of temperature change on the colloidal stability of a NP solution.

Question #3: What Determines the Final Particle Size? In case of monodispersity, the final particle size is determined by the number of particles to which the total amount of monomers (atoms) is distributed. The previous sections of this contribution revealed that for the Turkevich synthesis (which delivers monodisperse particles) the first two steps of the growth mechanism already determine the final particle number and therefore the final size. To understand what determines the final size, all decisive influences on this very short initial period need to be investigated.

General Considerations Regarding the Number of Seed Particles. As stated, the final size is defined by the total number of particles, which corresponds to the number of seed particles for the Turkevich synthesis. Figure 4a illustrates the two paths which in general determine the number of seed particles. (Note: Both can be relevant at the same time.) The first path comprises the amount of Au^0 which is available for the formation of the seed particles. It depends on the reduction chemistry during the process of seed particle formation. A larger amount of Au^0 leads to formation of

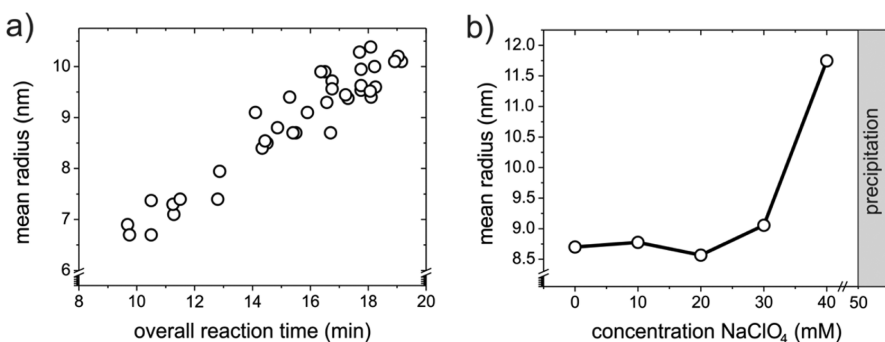


Figure 5. (a) Reproducibility study. Final mean radius *versus* overall reaction time for repetitions of the Turkevich standard synthesis (polydispersity = 10%). Repetitions were conducted over a period of one year. The overall reaction time was determined by observing the color change of the reaction solution until it shows a characteristic ruby red color. (b) Influence of ionic strength on standard Turkevich synthesis. Final mean radii *versus* total NaClO_4 concentration (for 0–30 mM, polydispersity = 10%; for 40 mM, polydispersity = 25%).

more seed particles. The total amount of gold is distributed to more particles. As a consequence, the final size is smaller. This is illustrated on the left side of Figure 4a.

The second path which influences the number of seed particles is the seed particle size. Larger seed particles consist of more Au^0 available for the seed particle formation and the final particle size is larger (illustrated on the right side of Figure 4a). Recently, a concept to describe nanoparticle growth governed by colloidal stability has been introduced and will be used within this discussion.³² In brief, colloidal stability is a result of attractive van der Waals and repulsive electrostatic forces between two particles. According to a theory by Derjaguin, Landau, Verwey, Overbeek (referred to as DLVO theory), the sum of these opposing forces results in a total interaction potential depending on the distance between two particles whereby the maximum is referred to as aggregation barrier.^{34,35} The aggregation barrier can be interpreted as an energy required for the aggregation of two particles which provides a measure for the colloidal stability. In general, the aggregation barrier (thus the colloidal stability) between two electrostatic stabilized particles increases with increasing particle size as illustrated in Figure 4b,c for identical particles. Herein, these curves (aggregation barrier *versus* particle size) are referred to as “stability curves”. The growth concept suggests that two particles can overcome the electrostatic repulsion and aggregate/coalesce as long as the aggregation barrier is lower than the thermal energy E_{KT} , thus enabling particles to grow (section I). In section II, the aggregation barrier cannot be overcome any longer inhibiting further particle growth. Simplified, the particle radius related to the intercept point of E_{KT} and the stability curve defines the minimum stable particle size. In the picture of the colloidal stability approach, the final particle size of a colloidal solution is therefore determined by the stability curve which depends on the surface charge and on the

chemical composition of the colloidal solution (e.g., specific nature of ions, ionic strength etc.) and by the available thermal energy E_{KT} . This approach provides an opportunity to describe the influences of reaction parameters on the size of particles. The concept was shown to be applicable for different nanoparticle syntheses which are based on a fast monomer supply (e.g., reduction of HAuCl_4 with NaBH_4).³⁶ Although the Turkevich synthesis comprises a weak reducing agent, the initial phase of seed particle formation can be described using this approach because monomers are provided relatively fast (see #2).

To summarize Figure 4, the reaction conditions of the Turkevich synthesis protocol can influence both, the colloidal stability of the seed particles and the chemistry of reduction during seed formation. Consequently, the reaction conditions determine the number of seed particles and therefore the final particle size. In fact, the final particle size is smaller the more seed particles are formed and *vice versa*.

Predominant Path for the Number of Seed Particles. The number of seed particles is determined by their colloidal stability and the chemistry of reduction during seed particle formation. In general, it is difficult to investigate these paths independently since most reaction conditions influence both of them at the same time. Therefore, a reproducibility study using only one set of reaction parameters (standard synthesis) is discussed first followed by an ionic strength variation study. Increasing the ionic strength by adding “unreactive” (noninvolved) ions does most likely influence the colloidal stability but not the reduction chemistry.

Reproducibility Study. For a reproducibility study with 40 repetitions, the Turkevich synthesis was performed by different scientists over a period of one year using different reactant solutions always strictly following the standard synthesis protocol. The final particle sizes were determined with SAXS. Figure 5a shows the final mean radii *versus* overall reaction time (time until precursor is reduced completely, determined by

observing the colloidal solution until it has a characteristic ruby red color). The final mean radii vary as much as from 6.5 to 10 nm (polydispersity = 10%). For small final radii (correspond to a larger number of seed particles), a shorter reaction time is observed. This indicates that the total surface area of the seed particles facilitates the kinetics of growth (steps 3 and 4). In other words, a decreasing final particle size is caused by an increasing number of seed particles, which in turn increases the kinetics of the steps 3 and 4. The deviation of final particle sizes might be surprising since an often mentioned advantage of the Turkevich synthesis is its high reproducibility.^{3,5,19,37} Nevertheless an extensive study has not been reported yet. In the presented picture of growth, either the reduction chemistry during seed particle formation, the colloidal stability of the seed particles or both are responsible for the lack of reproducibility. Following, it is shown that the colloidal stability has most likely a minor influence.

Influence of Colloidal Stability: Variation of Ionic Strength. Increasing the ionic strength of the reaction solution with NaClO₄ has no significant influence on the reduction chemistry since the added ions are "noninvolved" in chemical processes which are linked to the reduction of the gold precursor. Therefore, only the colloidal stability path (illustrated in Figure 4a) will change with different NaClO₄ concentrations. For the corresponding experiment, NaClO₄ was added to the Na₃Ct solution prior to mixing with HAuCl₄. The final particle sizes were determined with SAXS. Figure 5b displays the mean particle radius versus total concentration of NaClO₄ (referring to the final colloidal solution). No significant effect is observed up to 30 mM, which corresponds to a 120 times higher concentration compared to Au³⁺. Only at concentrations exceeding 30 mM larger AuNP are formed; above 50 mM, precipitation is observed. Similar observations were reported by Zhao *et al.* upon addition of NaNO₃.²¹

The relatively constant particle size for NaClO₄ concentrations of up to 30 mM reveals that the colloidal stability (and therefore the size of the seed particles) remains mostly unaffected for a wide range of ionic concentrations, in particular in the range of common Turkevich synthesis protocols. Although the colloidal stability of the seed particles plays an important role, it appears to be constant. Consequently, the deviations of final particle sizes observed in the reproducibility study are most likely not related to changes of the colloidal stability. Therefore, the reduction chemistry can be assumed to predominantly cause changes of the seed particle formation step and the number of particles.

Reduction Chemistry. From the results presented in Figure 5, it could be deduced that the chemistry of reduction during the first two steps has a considerable effect on the number of seed particles. Even apparent

small changes during the synthesis can influence the reduction to such a great extent that the final size differs significantly. The reaction chemistry of the solution is extremely complex since the reactants, citrate and gold ions, exist both in different chemical forms, which can be converted reversibly into each other. In addition, citrate can be oxidized irreversibly resulting in a variety of chemical species. This subsection discusses the chemistry of the reactants HAuCl₄ and Na₃Ct followed by an investigation of the decisive processes upon mixing.

Chemistry of the Gold Precursor. In the gold coordination sphere, four anions are coordinated in square planar geometry; at strong acidic conditions, these are four Cl⁻ ligands. With increasing pH value, the Cl⁻ ligands are exchanged successively by OH⁻ (see Figure 6, right side). At mild acidic, neutral, and mild alkaline conditions, mixtures of two or more gold complex species are obtained. Several researchers investigated the ratios between the different [AuCl_{4-x}OH_x]⁻ species with dependence on the pH value. The dominant gold complexes were determined (occasionally with different results) from quantitative analysis of the free Cl⁻ ligands using ion chromatography,³⁸ UV-vis and Raman spectroscopy,^{19,39,40} or by calculations from the pK values.^{28,41} In addition to the pH value, the ratio of the gold species is also known to be influenced by temperature.⁴¹ UV-vis spectra of a 0.25 mM HAuCl₄ solution at different temperatures (see Supporting Information SI-4) indicate, as expected, that elevated temperatures promote a shift of the equilibrium toward a more hydroxylated form. The redox potential of the gold complexes depends on the species.^{2,21,22,42} The concentration of species with higher redox potential ([AuCl₄]⁻) decreases with increasing pH.^{2,19,38,41,43} In addition to the redox properties, the actual gold species and thus also the pH value significantly influence the optical properties of the ionic gold solution. The [AuCl₄]⁻ complex exhibits two absorbance bands at ~226 and 313 nm, which can be assigned to the p_π → 5d_{x²-y²} and p_σ → 5d_{x²-y²} ligand–metal transition, respectively.^{19,38,40,41} The absorption bands decrease and blue-shift with exchange of Cl⁻ by OH⁻ ions (see Supporting Information SI-4). Therefore, the absorbance at 313 nm can be used to monitor the kinetics of the [AuCl_{4-x}OH_x]⁻ equilibrium. To study the temperature dependence of the establishment time of the gold complex equilibrium, NaOH was added to a 0.25 mM HAuCl₄ solution (pH = 3.3) at different temperatures to give a final pH of ~6.5 (equivalent to pH obtained by addition of 2.5 mM Na₃Ct), while the absorbance at 313 nm was recorded time-resolved. Selected data can be found in Supporting Information SI-4. Figure 6a depicts the time to establish the complex equilibrium versus temperature. For 95 °C (boiling conditions are not accessible due to experimental limitations), the equilibrium is

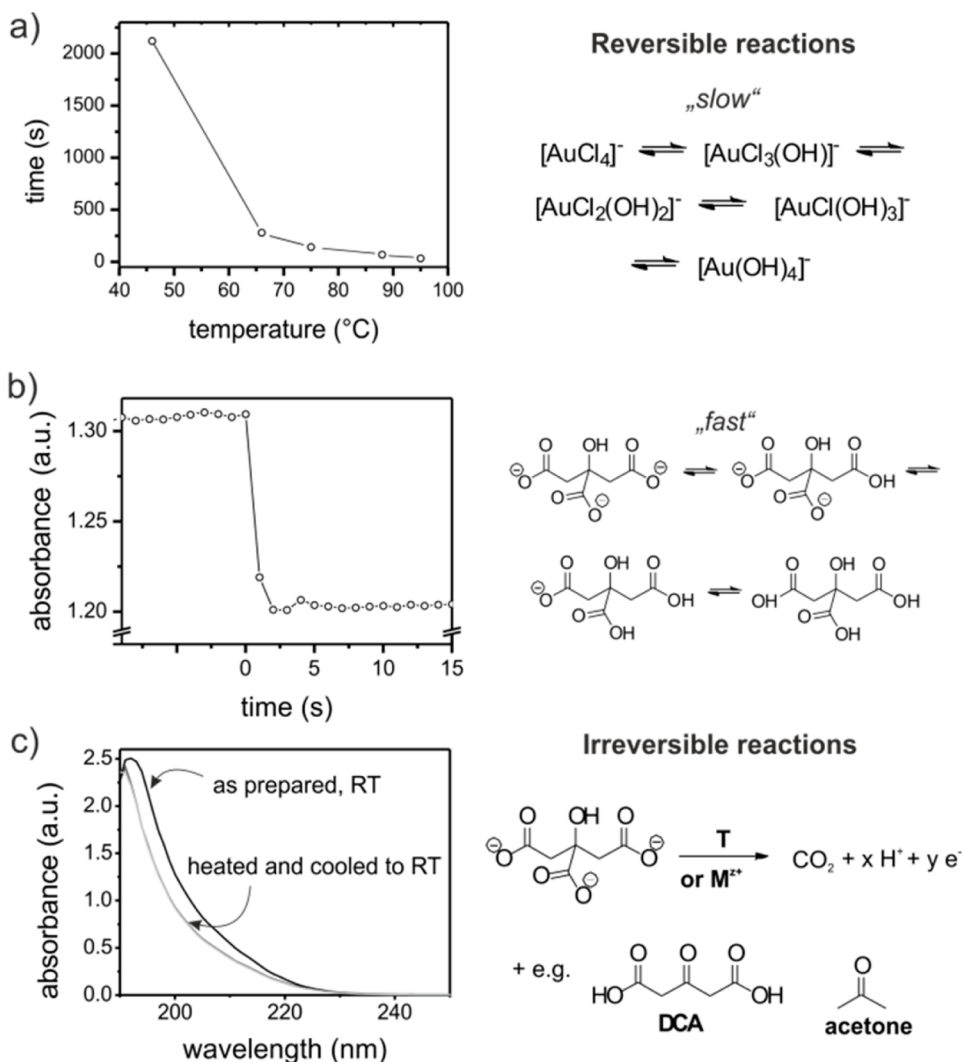


Figure 6. Chemical reactions of the pure reactants and their kinetics. (a) Time until gold complex equilibrium (see right side) is reached in a 0.25 mM HAuCl_4 solution upon addition of NaOH to give a final pH of ~ 6.5 . The equilibrium time was determined at different temperatures. (b) Absorbance at 200 nm for a 1.25 mM citrate solution at 23 °C upon addition of HCl to give a final pH of ~ 6.5 . The pH value influences the protonation equilibrium of citrate as illustrated on the right side. (c) UV-vis spectrum of 1.25 mM citrate solutions recorded as prepared and spectra of the same solution heated to 30 and 60 °C, respectively, and cooled to 23 °C. The latter spectra are identical.

reached after ~ 30 s. The equilibrium time for the gold complexes increases significantly with decreasing temperature.

Chemistry of the Reducing Agent. Similar to the gold complex, different citrate species exist in a chemical equilibrium (see Figure 6, right side). Citrate has three carboxyl groups, which can be protonated/deprotonated, leading to an acid–base buffer. The ratio of the different citrate species in dependence of the pH can be estimated from their pK_a values (3.2, 4.8, and 6.4).^{22,28} At low pH values, the fully protonated form is favored. Citrate shows no absorbance in the visible region (colorless solution) but absorbs light in the UV range. The optical properties change with protonation/deprotonation (see Supporting Information SI-4). Therefore, the absorbance at 200 nm can be used to monitor the kinetics of the protonation

equilibrium upon addition of H^+ . To avoid saturation effects of the detector, the concentration was decreased to $[\text{Na}_3\text{Ct}] = 1.25$ mM (pH 7.6). HCl was added in an amount equivalent to 0.125 mM HAuCl_4 (to keep a molar ratio of 10:1 as in the standard synthesis) to decrease the pH to 6.44. Figure 6b depicts the absorbance (200 nm) versus time upon addition of HCl at 23 °C. The kinetics at elevated temperatures are not accessible with a standard UV–vis setup. Within ~ 2 s, the absorbance decreases to a constant level indicating that the protonation equilibrium is reached relatively fast. Similar to the ligand exchange equilibrium of the gold complexes, the protonation equilibrium of citrate is temperature-dependent (see Supporting Information SI-4). In addition, the irreversible oxidation of citrate to dicarboxy acetone (DCA),^{3,6,22,23,44–46} acetone or other products⁴ upon heating or in the presence

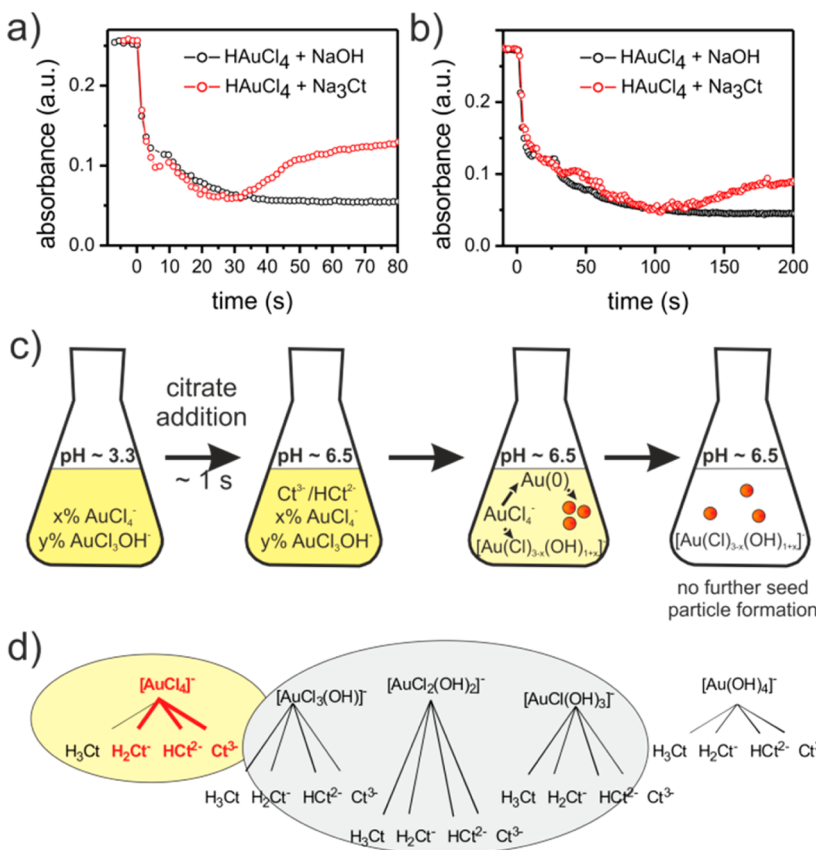


Figure 7. Chemistry and kinetics upon mixing the reactants HAuCl₄ and Na₃Ct. Absorbance at 313 nm of a 0.25 mM HAuCl₄ solution upon addition of 2.5 mM Na₃Ct or NaOH to reach a final pH of ~6.5 at (a) 95 °C and (b) 75 °C; (c) sketch of chemical processes during seed particle formation. (d) Theoretically possible combinations of gold complex and citrate species. The yellow background designates combinations which are most likely to supply Au monomers during the seed particle formation. The gray background designates combinations which are most likely to supply Au monomers during steps 3 and 4 of the growth mechanism. Note that not all listed combinations can co-occur in a Turkevich synthesis.

of metal ions has been described in the literature. The formation of DCA has been assumed to play a decisive role for the mechanism of the Turkevich synthesis^{3,6,12,23,46} which will be discussed later in this contribution. However, a threshold temperature for the formation of citrate oxidation products has not been reported so far. Figure 6c shows UV-vis spectra of 1.25 mM citrate solutions recorded at 23 °C as prepared and heated to 30 and 60 °C before, respectively. The data indicates that the citrate solution is changed irreversibly, most likely attributed to a decomposition pathway, already upon heating to 30 °C.

In summary, both reactants of the Turkevich synthesis exist in a variety of different species. Temperature and pH value determine the actual ratios of the species. The ligand exchange equilibrium of the gold complexes upon increasing the pH value is reached much slower compared to the protonation equilibrium of citrate upon addition of H⁺. Irreversible oxidation products of citrate are formed already at temperatures slightly above room temperature.

Chemistry upon Mixing HAuCl₄ and Na₃Ct. The investigations of the pure HAuCl₄ and Na₃Ct show that the reactant solutions can contain a variety of chemical

species already before mixing. Upon addition of Na₃Ct to HAuCl₄, the pH increases and shifts the gold complex equilibrium toward more hydrolyzed forms. In addition, oxidation products of citrate are formed. All these processes create a continuously changing Turkevich reaction system with a great complexity and a variety of possible pathways for the reduction of Au³⁺. Recently, a molecular reduction mechanism was proposed which comprises at first a ligand exchange of the precursor with a citrate ion to form an intermediate gold complex, a ring closure step followed by a concerted decarboxylation, the reduction of the Au³⁺-complex to an Au⁺-complex and a disproportionation step which finally leads to atomic Au.² In fact, 20 different combinations of gold and citrate species are possible (see Figure 7d). Of course, not every combination makes sense from a chemical point of view (e.g., co-occurrence of [Au(OH)₄]⁻ and H₃Ct) or regarding the given reaction conditions (pH values range only from ~3.3 to 7 in the standard Turkevich synthesis). Nevertheless, several potential reaction pathways involving different chemical species are available for the reduction process. In a recent publication, DFT calculations for three selected combinations of gold and

citrate species were made.²⁸ The reduction was found to be facilitated for $[\text{AuCl}_4]^-$ and highly deprotonated citrate ions with the gold species having the major impact on the total reaction free energy. The herein discussed growth mechanism of the Turkevich synthesis demands that at least one process stops the seed particle formation. Most likely, this process is associated with the transformation of the reactant species in the beginning of the synthesis. A simple analytical method to determine the change of chemical composition during the seed particle formation phase is not available. Nevertheless, time-resolved monitoring of the 313 nm absorbance upon mixing the reactants can deliver useful insights since the $[\text{AuCl}_4]^-$ species shows a significant absorbance at this wavelength while the $[\text{AuCl}_3\text{OH}]^-$ species does only slightly absorb at this wavelength. Figures 7a,b show the absorbance (313 nm) versus time for 95 and 75 °C, respectively, for mixing HAuCl₄ and Na₃Ct (standard concentrations) and mixing HAuCl₄ and NaOH (to reach the same final pH of ~6.5). For both investigated temperatures, the curve profiles are almost the same in the beginning. For 95 °C, the seed particle formation phase can be assigned approximately to the first 30 s of the synthesis (see #2) matching the phase during which the curve profiles are almost the same. Therefore, it can be expected that the gold equilibrium is shifted from $[\text{AuCl}_4]^-$ to $[\text{AuCl}_{3-x}(\text{OH})_{1+x}]^-$ during the seed particle formation phase. More indication comes from an UV-vis study with varied initial concentration of gold precursor (see #3 and Supporting Information SI-5). Figure 7c illustrates the most probable chemical processes during the seed formation step. Before mixing, the HAuCl₄ solution contains a certain amount of $[\text{AuCl}_4]^-$ ions (pH 3.3). Upon addition of citrate, the pH value increases almost immediately to ~6.5, which shifts the equilibrium to a less reactive gold complex (causing discoloring of the reaction solution). A small fraction of reactive $[\text{AuCl}_4]^-$ can be reduced quickly within this time supplying Au⁰ for the seed particle formation. As soon as the equilibrium is reached, the solution contains mainly or only $[\text{AuCl}_{3-x}(\text{OH})_{1+x}]^-$ species which are not reactive enough to be reduced fast in solution. Instead, these species are attracted by the seed particles, enriched in their EDL which leads to a reduction at the seed particles' surfaces. The seed-mediated growth mechanism is basically a fortunate coincidence and the consequence of a favorable interaction of many circumstances. The chemically induced transformation of a reactive precursor species into a less reactive species (which itself is a lucky circumstance) happens just in appropriate time to trigger the fast generation of a small but sufficient amount of monomers to form seed particles. Just as important, the transformation of $[\text{AuCl}_4]^-$ to $[\text{AuCl}_{3-x}(\text{OH})_{1+x}]^-$ blocks a further fast supply of monomers in solution which could form further particles or grow onto existing particles in an uncontrolled way.

existing particles in an uncontrolled way at later reaction times.

Role of Dicarboxyacetone (DCA). Regarding the reduction process, some publications deduced a special role for DCA. Turkevich and co-workers found DCA to be a kinetically faster reducing agent for HAuCl₄ than citrate and assigned the origin of the "induction period" (initial phase during which they could not observe the formation of particles) to the formation of DCA from citrate.^{6,12} In their interpretations, DCA organizes the gold ions into large macromolecules. The large local concentration of gold precursor was supposed to facilitate the reduction of Au³⁺. Later, DCA was supposed to form a DCA–Au⁺ complex facilitating selectively the disproportionation step of Au⁺ to Au⁰.^{2,3} However, Doyen *et al.* could not find experimental support for the existence of such an intermediate from NMR investigations.⁴ To investigate the influence of DCA with regard to the growth mechanism, a series of experiments were carried out (i) with DCA used as the only reducing agent instead of Na₃Ct, (ii) DCA added to a standard synthesis after seed particle formation, and (iii) DCA added to Na₃Ct before mixing with HAuCl₄. Experimental details, results and discussion can be found in Supporting Information SI-6. From the experimental results, it can be concluded that large concentrations of DCA (~40% with respect to citrate concentration) if present already during the seed particle formation change the growth mechanism. The concentration of DCA during the seed particle formation step is rather low in a standard Turkevich synthesis. Therefore, DCA plays no essential role in the reduction mechanism of the seed particle formation (*i.e.*, steps 1 and 2). However, high concentrations of DCA during steps 3 and 4 accelerate the autocatalytic growth of the seed particles but do not affect the final particle size. Consequently, DCA has no significant influence on the final particle size for common Turkevich synthesis protocols.

Summary #3. The seed-mediated growth mechanism of the Turkevich synthesis ensures the formation of highly uniform AuNP. To understand what determines the final particle size, the general mechanism (see #1) has to be extended as illustrated in Figure 8. The seed-mediated growth mechanism is a fortunate coincidence created by a favorable interplay of different chemical processes. Upon mixing the reactants, the buffer effect of Na₃Ct induces the transformation of reactive $[\text{AuCl}_4]^-$ species into less reactive $[\text{AuCl}_{3-x}(\text{OH})_{1+x}]^-$ species. This process occurs in just appropriate time to trigger the fast generation of a small but sufficient amount of monomers from $[\text{AuCl}_4]^-$ to form stable particles, the seed particles. The transformation of the reactive gold complex blocks a further fast supply of monomers in solution which could form further particles or grow onto existing particles in an uncontrolled way. Therefore, the shift

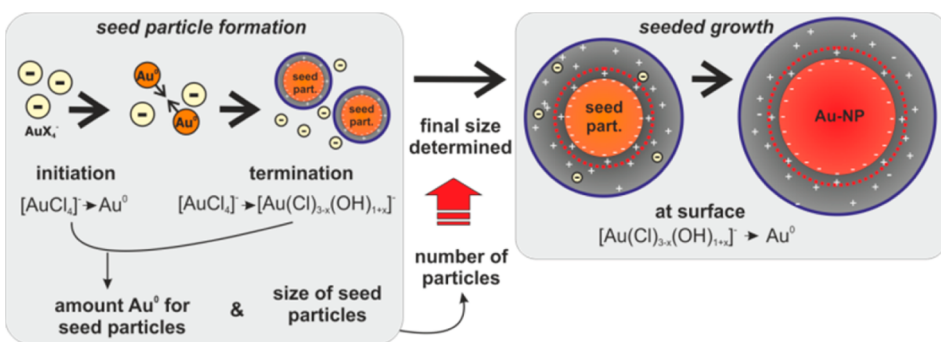


Figure 8. Summary of growth process and the underlying chemical processes.

of the gold complex equilibrium terminates step 1 of the growth mechanism. The kinetics of the transformation of $[\text{AuCl}_4]^-$ to more hydrolyzed forms and the kinetics of the reduction of $[\text{AuCl}_4]^-$ to Au^0 determine the amount of monomers available for seed particle formation. The size of the seed particles defines how many particles can be formed from the available Au^0 monomers. The resulting number of seed particles corresponds to the final particle number and determines the final size since residual gold grows exclusively onto the seed particles. Certainly, the described processes are even more complex than illustrated in Figure 8. However, the essential points summarized herein allow an understanding of parameter influences on the growth mechanism and the final particle size.

Question #4: How Do Synthesis Parameters Influence the Particle Growth and Therefore the Final Size? The influence of reaction conditions on the final particle size and the subsequent development of synthesis protocols are subject of many publications. However, an understanding of how the parameters influence the final size is still missing. In the following section, results of parameter variations described in literature in combination with further parameter studies are discussed using the gained knowledge from sections #1–3. As shown in #3, the synthesis is not as reproducible as often stated. This is most likely caused by small differences of the reduction process during the seed particle formation which are difficult to control in a typical laboratory environment. Therefore, all parameter studies described herein were, as far as possible, carried out within a short period of time.

Variation of Reactant Concentrations. The variation of reactant concentrations is the common adjustment of a synthesis recipe. Table 1 summarizes the results of a parameter study following the standard Turkevich protocol. For two Na_3Ct concentrations (2.5 and 3.75 mM), the HAuCl_4 concentration was varied (0.125, 0.25 and 0.5 mM). Each experiment was repeated three times. The effect of Na_3Ct concentration is negligible, while the final size decreases significantly for higher HAuCl_4 concentrations.

Variation of Citrate Concentration. Kumar *et al.*²³ summarized the results of different publications on the

variation of the Na_3Ct concentration at a fixed gold concentration (~ 0.25 mM) using the work of Turkevich,⁶ Chow and Zukoski,⁹ Freund,¹⁰ Spiro¹⁰ and Frens.⁸ Kumar's overview shows that the final size remains almost unaffected for a wide range of Na_3Ct concentrations, which is also congruent with results by Takiyama¹⁴ and those presented herein in Table 1. Only for very small (approximately below 0.5 mM) or very high (10 mM) citrate concentrations, the final size as well as the polydispersity were shown to increase.^{19,23}

The results can be explained by the different roles of the citrate species, which include reducing agent, stabilizer and pH mediator. As shown in #3, the buffer effect of citrate shifts the gold complex equilibrium toward less reactive forms upon mixing so that the seed particle formation is stopped. This process is required to create the fortunate coincident of the seed-mediated growth mechanism. If citrate is added in a sufficient concentration, the kinetics of the protonation equilibrium and the final pH of the solution are approximately the same irrespective of the molar excess.¹⁹ Therefore, the seed particle formation is almost not affected by an increasing citrate concentration leading to final particles of about the same size. If citrate is added in very low concentration, the molar excess might still be sufficient to reduce the amount of Au^{3+} but not to shift the gold complex equilibrium from reactive $[\text{AuCl}_4]^-$ to less reactive hydrolyzed forms. The fortunate coincident vanishes and, in addition to the reduction of Au^{3+} in the EDL of preformed particles, reduction can also occur unselectively during the entire synthesis. This produces nonuniform polydisperse final colloids. Furthermore, Na_3Ct plays a decisive role in stabilizing the initially formed particles. For very low concentrations, seed particles which still might exist have to grow to larger sizes to reach a stable size (see Figure 4b, curve A versus B). For very high citrate concentrations (see Chow and Zukoski⁹), the Turkevich synthesis can be expected to follow the seed-mediated growth mechanism, but the colloidal stability of the seed particles decreases due to the high ionic strength. The seed particle size increases leading to less particles and larger final sizes (similar to the NaClO_4 addition experiment in #3).

TABLE 1. Variation of HAuCl₄ Concentration for Two Different Concentrations of Na₃Ct (2.5 and 3.75 mM)^a

	0.125 mM HAuCl ₄ pH = 3.6	0.25 mM HAuCl ₄ pH = 3.3	0.5 mM HAuCl ₄ pH = 3.0
[Na ₃ Ct] = 2.5 mM			
Final size	13.8 ± 1.2 nm	9.3 ± 0.4 nm	5.5 ± 0.1 nm
Molar Ratio Ct:Au	R = 20	R = 10	R = 5
Overall reaction time	19:27 ± 1:30 min	15:30 ± 0:55 min	3:00 ± 0:10 min
Relative particle number	0.2	1	9.7
[Na ₃ Ct] = 3.75 mM			
Final size	14.2 ± 2.1 nm	9.8 ± 0.5 nm	5.3 ± 0.7 nm
Molar Ratio Ct:Au	R = 30	R = 15	R = 7.5
Overall reaction time	17:45 ± 0:25 min	14:30 ± 0:10 min	4:30 ± 0:15 min
Relative particle number	0.2	1	12.6

^a Average mean radii (polydispersity = 10%) were calculated from three separated experimental runs. The relative particle number was calculated with respect to the 0.25 mM standard concentration of HAuCl₄ (r.n. = $\langle r_1 \rangle^3 / \langle r_2 \rangle^3 \cdot [HAuCl_4]_2 / [HAuCl_4]_1$, see also Experimental Section).

Variation of HAuCl₄ Concentration. Kimling *et al.* investigated the influence of HAuCl₄ concentration on the final size distribution for up to 1.2 mM.⁵ However, size trends are difficult to deduce from the presented data. Li *et al.* varied the HAuCl₄ and Na₃Ct at fixed molar ratios and found the mean particle radius to decrease slightly for increasing HAuCl₄ concentration (0.25–1.5 mM).⁴⁷ Takiyama observed a clear decrease of particle size with increasing HAuCl₄ concentration (0.1–1 mM).¹⁴

For the study presented in Table 1, the citrate concentration was held constant (2.5 and 3.75 mM, respectively), while the HAuCl₄ concentration was adjusted to 0.125, 0.25, and 0.5 mM. The citrate concentrations were chosen sufficiently high to create the fortunate coincident and ensure a seed-mediated growth mechanism for all syntheses. The study shows that the final particle radius is significantly smaller for increasing precursor concentration. The origin of the observed trend becomes apparent from comparing the pH values of the initial HAuCl₄ solutions which depend on the precursor concentration. The pH value of HAuCl₄ varies between 3.6 (0.125 mM) and 3.0 (0.5 mM). Supporting Information Figure SI-4d shows the absorbance at 313 nm (characteristic maximum for [AuCl₄]⁻) versus the pH of a 0.25 mM precursor solution. The absorbance decreases significantly between pH 2 and 4 which indicates that the ratio of [AuCl₄]⁻ / [AuCl_{4-x}(OH)_x]⁻ decreases in less acidic medium. During the seed particle formation step, mainly the reduction of the reactive [AuCl₄]⁻ species provides Au⁰ monomers for the seed particle formation. Therefore, if the initial concentration of [AuCl₄]⁻ is higher, more monomers can be provided and more seed particles are formed resulting in smaller final particles (*cf.* chemistry of reduction path in Figure 4a). An additional study with time-resolved UV-vis measurements and a more detailed discussion can be found in Supporting Information SI-5. For example, using a 0.5 mM

HAuCl₄ solution, which contains more initial [AuCl₄]⁻ than the standard 0.25 mM solution, about 13 times more seed particles are formed leading to smaller final particles. This results in a larger total surface area available for growth steps 3 and 4 (*cf.* reproducibility study in #3). As a result, the overall reaction time decreases with increasing HAuCl₄ concentrations.

Summary #4.1. The concentration of citrate has almost no effect on the final size as long as its buffer capacity ensures a neutral pH after mixing the reactants. This provides a shift of the gold complex equilibrium toward less reactive forms to create the fortunate coincident which is required for the seed-mediated growth mechanism. In contrast, the concentration of HAuCl₄ has a significant influence since it determines the initial pH value of the precursor solution and the ratio of [AuCl₄]⁻ / [AuCl_{4-x}(OH)_x]⁻ during seed particle formation. For higher HAuCl₄ concentrations, a larger percentage of [AuCl₄]⁻ is available during the seed particle formation. More particles are formed. Therefore, smaller particles are obtained for higher precursor concentrations.

Order of Reactant Addition. Recently, it was reported that the order of reactant addition influences the final particle size.^{3,46} In the standard synthesis, a Na₃Ct solution is added to a preheated HAuCl₄ solution. In contrast, the inverse method corresponds to the addition of a small volume of highly concentrated HAuCl₄ solution to a large volume of diluted preheated Na₃Ct solution. The final concentrations of both reactants are retained. It was found that final particle size and synthesis time decrease using the inverse method. Ojea-Jiménez *et al.* assigned this observation to the formation of DCA by thermal oxidation of citrate during preheating of the reducing agent solution. They suggested that the formation of DCA–Au⁺ complexes facilitates the disproportionation to Au⁰ leading to fast nucleation and small particles.³ Sivaraman *et al.*

assigned the influence of inverse reactant addition to the formation of DCA, too. However, they pointed out that thermal citrate oxidation during preheating is unlikely to produce a sufficient amount of DCA. It was concluded that chemical oxidation of citrate by Au^{3+} is favored in the inverse method producing more DCA during the initial phase of the reaction.⁴⁶

We repeated the inverse experiment three times and found the final size to be smaller ($7.6 \pm 0.1 \text{ nm}$) and the reaction time ($670 \pm 20 \text{ s}$) to be shorter for the inverse method compared to the standard method, congruent to the previous reports. It was shown in #3 that a Na_3Ct solution is changed irreversibly upon heating, most likely due to the formation of oxidation products such as DCA. However, it was also shown that DCA has no significant influence on the growth mechanisms and thus the final size even when added in high concentrations (1 mM) prior to the reaction. Therefore, even if DCA is formed during the preheating step in the inverse method, it is unlikely that its concentration is high enough to influence the growth mechanism and the reaction outcome. Instead, the effect of the inverse method can be attributed to different initial amounts of reactive $[\text{AuCl}_4]^-$ similar to the variation of HAuCl_4 concentration discussed in the previous subsection. The gold equilibrium was shown to be shifted to more hydrolyzed forms with increasing temperature. Preheating of the gold precursor solution (standard method) leads to less initial $[\text{AuCl}_4]^-$. In addition, the concentration of HAuCl_4 in the inverse method is very high (50 mM). The corresponding low pH value provides the presence of even more $[\text{AuCl}_4]^-$ during seed particle formation. Consequently, more Au^0 is available for the seed particle formation and more particles are formed in the inverse method (cf. chemistry of reduction path in Figure 4a). This leads to smaller final particles as well as to a shorter reaction time since the total surface area of the seed particles is higher facilitating a fast growth during steps 3 and 4.

Summary #4.2. The inverse method comprises the change of reactant addition order and leads to the formation of smaller particles. This effect is caused by different initial amounts of $[\text{AuCl}_4]^-$ available during seed particle formation rather than by any DCA induced processes as assumed previously.

pH Value. The important role of citrate as pH mediator which is essential to ensure a seed-mediated growth mechanism was already pointed out. Obviously, the pH value has a significant effect on the final size. The acidity influences the initial amount of $[\text{AuCl}_4]^-$, the buffer capacity of citrate, the colloidal stability of the seed particles and the reducing power of citrate. Indeed, Patungwasa *et al.* reported that the pH value influences size, polydispersity and morphology of the final particles.²² Zhao *et al.* and Ojea-Jiménez and Campanera showed that the final

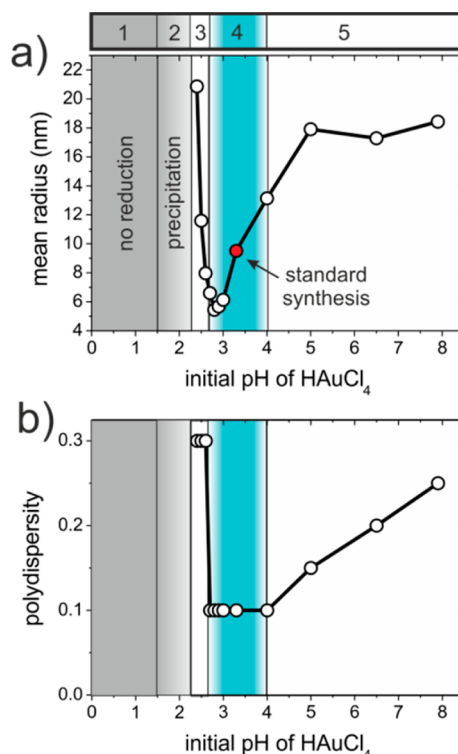


Figure 9. Influence of the initial pH value of the HAuCl_4 solution. (a) Final mean particle radii, (b) polydispersities.

particles are smaller for more acidic conditions.^{21,28} It was also reported that the total reaction time decreases significantly at low pH values.^{19,28} Figure 9 shows the results of a parameter study for which the initial pH value of the 0.25 mM HAuCl_4 (unmodified pH = 3.3) solution was adjusted prior to mixing with Na_3Ct adding either HCl or NaOH. As suggested above, the pH value can have several influences creating a complex interplay of different processes. For a clearer discussion of the results, the graph shown in Figure 9 is divided into five areas.

For $\text{pH} < 1.5$ (area 1), no reduction of the gold precursor is observed. The high concentration of H^+ exceeds the buffer capacity of citrate which becomes fully protonated upon mixing with HAuCl_4 . Pure H_3Ct cannot reduce any Au^{3+} species since the formation of an intermediate complex with the gold ion (first step of molecular reduction mechanism²⁸) requires at least one deprotonated carboxy group.

In area 2 ($1.5 < \text{pH} < 2.3$), Au^{3+} is reduced to Au^0 , but only macro sized particles which precipitate at the container walls are formed. The observation can be explained by the effect of ionic strength which is extremely high in area 2 due to the addition of HCl in large amounts. Colloidal solutions are not stable (cf. colloidal stability path in Figure 4a).

Areas 3 and 5 are complex since the seed-mediated growth mechanism is not retained. For a better understanding, area 4 is discussed first. Area 4 comprises only very slight acidifying/alkalizing of the initial HAuCl_4

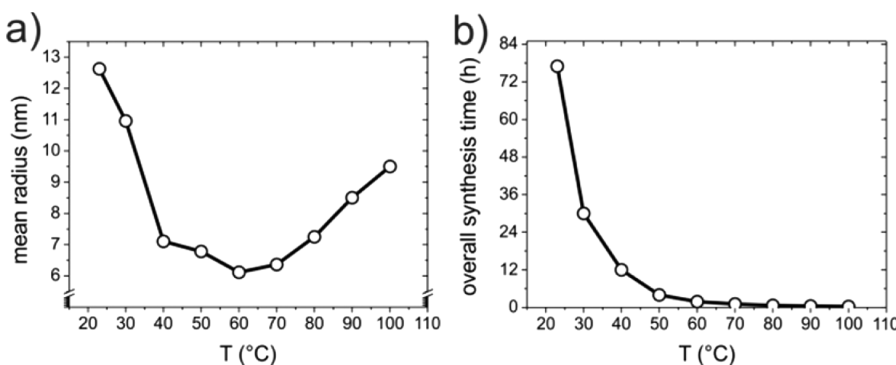


Figure 10. Results of temperature variation study. (a) Mean radii (polydispersity = 25% at 20 °C, 20% at 30 °C, rest 10%). (b) Overall synthesis time versus temperature determined by observing the color change of the reaction solution.

solution (pH 2.7–4) so that the prerequisites for the fortunate coincident are fulfilled facilitating a seed-mediated growth mechanism. First, enough $[\text{AuCl}_4]^-$ is present in the initial precursor solution to trigger the seed particle formation. Second, the buffer capacity of Na_3Ct is sufficient to shift the gold complex equilibrium upon mixing (terminating the seed particle formation). As a result of the retained seed-mediated growth mechanism, the obtained solutions are relatively uniform (polydispersity 10%). A minimum mean radius of $r=5.4$ nm is obtained at pH = 2.8. The final size increases with increasing pH value which is attributed to the initial ratio $[\text{AuCl}_4]^-/[\text{AuCl}_{4-x}(\text{OH})_x]^-$ as already discussed in detail before (see Variation of HAuCl₄ Concentration).

Within areas 3 and 5, the presented seed-mediated growth mechanism is not retained and the final particles are rather polydisperse. The reasons for the changed growth mechanism are different. In area 3, the buffer capacity of Na_3Ct is not sufficient to stop the seed particle formation. In contrast, in area 5 the initial concentration of $[\text{AuCl}_4]^-$ is too low to trigger the fast formation of seed particles. For both areas, the growth mechanism can be expected to be “mixed”. Seed particle formation might still occur but simultaneously uncontrolled growth of existing and formation of further particles can take place. The growth mechanism is most likely “less and less” seed-mediated. In addition, the ionic strength increases the more HCl or NaOH is added to the initial HAuCl₄ solution. The colloidal stability of the seed particles (if present) and the final particles decreases which leads to larger particle sizes (cf. colloidal stability path in Figure 4a).

The variation study with pH-adjustment of the HAuCl₄ solution prior to the synthesis illustrates the complexity of the processes which determine the final size. Another possibility of pH variation is a change subsequent to the mixing of the reactants. Shiba *et al.* added NaOH to the reaction solution after different delay times.⁴² They showed that the final size is larger if NaOH is added very quickly after mixing HAuCl₄ and Na_3Ct compared to a later addition. This observation

can be explained by accelerating the gold equilibrium shift toward hydrolyzed forms by addition of NaOH. The seed particle formation is stopped earlier the sooner NaOH is added to the mixture. Less seeds can be formed (cf. chemistry of reduction path in Figure 4a) resulting in larger final particles.

Summary #4.3. The impact of the pH value on the Turkevich synthesis is enormous. The acidity determines whether the seed-mediated growth mechanisms can actually occur. The fortunate coincident vanishes if the gold precursor solution is too acidic and exceeds the buffer capacity of citrate. It also vanishes for too high pH values since the initial amount of reactive $[\text{AuCl}_4]^-$ is too low to trigger the fast formation of seed particles. As a consequence of the changed growth mechanism, the reduction of Au^{3+} can occur unselectively leading to nonuniform particles for very acidic or neutral reaction conditions. In addition, the pH value influences the initial amount of $[\text{AuCl}_4]^-$ available during seed particle formation. More seed particles are formed in more acidic HAuCl₄ solutions. Furthermore, the colloidal stability decreases with addition of HCl or NaOH (ionic strength increases) leading to a larger final size. It also has to be noted that the reducing power of citrate is lost at extremely acidic conditions. The minimum size for standard conditions is obtained at pH(HAuCl₄) = 2.8 which leads to particles with a mean radius of $r = 5.4$ nm.

Synthesis Temperature. The synthesis temperature has been investigated only occasionally yet. Turkevich *et al.* reported that the final size decreases for a synthesis temperature of 80 °C.⁶ In addition, the overall synthesis time was found to be longer at lower temperatures.^{6,47} Takiyama conducted an elaborated temperature study for which he also varied the initial HAuCl₄ concentration at each investigated temperature. He observed a decreasing final size for changing the synthesis temperature from 100 to 80, 70, and 60 °C. In Figure 10, the results of a temperature study following the standard synthesis are displayed. The HAuCl₄ solution was heated to the according synthesis temperature for 15 min before adding the citrate solution. Particles

synthesized at room temperature are rather polydisperse and large ($r = 12.6$ nm, polydispersity = 25%). The particle size decreases with increasing synthesis temperature and reaches a minimum at 60 °C ($r = 6.1$ nm, polydispersity = 10%). Further temperature increase results in larger particles. The synthesis accelerates significantly with increasing temperature (see Figure 10b).

Similar to the pH value, the temperature influence on the final size is very complex. The kinetics of the chemical processes which determine the amount of Au^0 during seed particle formation are temperature-dependent. The gold complex equilibrium is also influenced by temperature which changes the initial amount of reactive $[\text{AuCl}_4]^-$ (cf. chemistry of reduction path in Figure 4a). In addition, the seed particle size depends on temperature (cf. colloidal stability path in Figure 4a).

As discussed in #3, two chemical processes influence the amount of Au^0 available for seed particle formation. The transformation kinetics of $[\text{AuCl}_4]^- \rightarrow [\text{AuCl}_{3-x}\text{OH}_{1+x}]^-$ determine the time frame during which Au^0 can be produced for seed particle formation. The kinetics of the reduction $[\text{AuCl}_4]^- \rightarrow \text{Au}^0$ determine which amount of monomers is supplied during this time frame. Both processes become faster with increasing temperature. In other words, the time frame of the seed particle formation step becomes shorter with increasing temperature, but $[\text{AuCl}_4]^-$ is also reduced faster during the available time. Due to these opposing tendencies, the amount of Au^0 available for seed particle formation will vary with temperature. As stated, another temperature influence that needs to be considered is the shift of the gold equilibrium. The initial ratio of reactive $[\text{AuCl}_4]^-$ decreases at higher temperatures (see Supporting Information SI-4) which contributes to a decreasing amount of available Au^0 for seed particle formation. The temperature also influences the seed particle size. The concept to describe nanoparticle growth via colloidal stability as presented in #3 can be used to illustrate this influence. Higher temperatures increase the thermal energy E_{KT} of the reaction system. The intersection of E_{KT} and stability curve, which is associated with the minimal stable particle radius, is obtained for larger particle sizes (see Figure 4c). This temperature effect on particle size has been shown previously for AuNP obtained by NaBH_4 reduction.³⁶ Therefore, for a defined Au^0 amount, an increasing temperature leads to the formation of larger and fewer seed particles. At last, it has to be noted that the principle growth mechanism might change for low temperatures (around room temperature). At these temperatures, too few Au^0 monomers might be formed in the initial phase to form a sufficient amount of seed particles. Other pathways which can comprise the reduction of $[\text{AuCl}_{3-x}\text{OH}_{1+x}]^-$ species in solution might also occur. The result is a nonuniform polydisperse solution as obtained for

20 and 30 °C. The combination and interplay of the different described tendencies leads to a nonlinear curve shape for final size versus synthesis temperature.

Summary #4.4. The significant temperature influence on the final size is derived from a combination of processes. For increasing temperatures, the time frame for the seed particle formation becomes shorter. The reduction of $[\text{AuCl}_4]^-$ during the available time is accelerated at higher temperatures which enhances the supply of Au monomers. Since the gold complex equilibrium is temperature-dependent, the ratio of initial $[\text{AuCl}_4]^-$ decreases at higher temperatures facilitating the formation of less Au^0 and less particles. In addition, the seed particle size is larger for higher temperatures, also resulting in the formation of less seed particles. The interplay of all described processes leads to the measured nonlinear temperature dependence with a size minimum at 60 °C ($r = 6.1$ nm).

Question #5: Why Does the Citrate Reduction of Silver Nitrate (AgNO_3) Not Result in Monodisperse and Uniform Particles as for HAuCl_4 ? Inspired by the Turkevich synthesis, Lee and Meisel used Na_3Ct to prepare silver nanoparticles (AgNP) by the chemical reduction of aqueous AgNO_3 .⁴⁸ In contrast to the Turkevich synthesis, the AgNP obtained by Lee–Meisel are much larger ($r = 30$ –100 nm) with a high polydispersity and with different morphologies.⁴⁹ Spherical particles can only be obtained using a stepwise reduction method.⁵⁰ The Lee–Meisel method was investigated by recording UV–vis spectra at different reaction times.^{50–52} In the beginning, no absorbance is detectable. After approximately 1/3 of the total reaction time, a plasmon band is observed which increases during the course of the reaction indicating the growth of AgNP. Gorup *et al.* quenched the particle growth by addition of ammonia after first appearance of a plasmon absorbance (the residual Ag^+ forms a stable $[\text{Ag}(\text{NH}_3)_2]^+$ complex). They detected AgNP with average radius of 1.1 nm as apparent from SEM imaging.⁵¹ Nevertheless, it cannot be excluded that these small particles were formed from unreacted precursor residues on the substrate reduced by the electron beam. In general, the growth mechanism of the Lee–Meisel synthesis is rather unclear.

To investigate the Lee–Meisel synthesis, time-resolved SAXS measurements using a free-liquid jet setup were conducted at beamline ID02 (ESRF). The synthesis was carried out with concentrations of $[\text{AgNO}_3] = 0.25$ mM and $[\text{Na}_3\text{Ct}] = 2.5$ mM at 85 °C (total reaction time ~70 min). The SAXS experiment was conducted twice using different sample to detector distances to measure the scattering in the lower and larger \mathbf{q} -scale. The two separated SAXS measurements were necessary to investigate the formation of smaller particles (demands higher \mathbf{q} values, see Figure 11a) and the growth of larger particles (demands very small \mathbf{q} values, see Figure 11b). In the first 25 min of the reaction, no particle scattering could be detected. The origin of this induction period

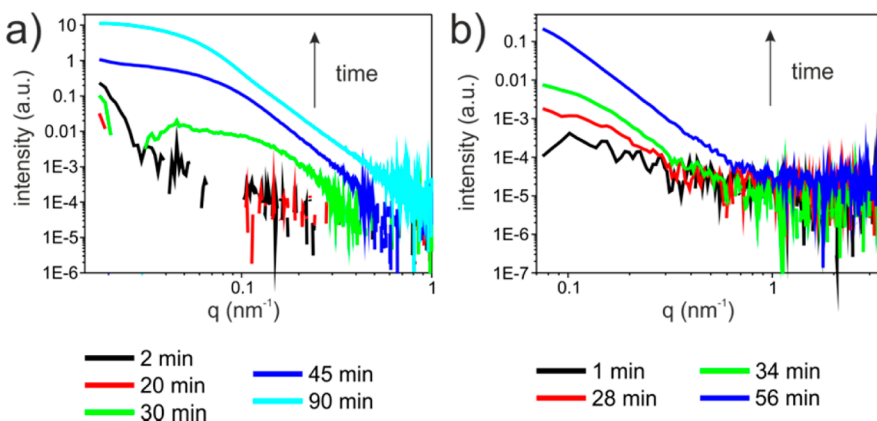


Figure 11. Time-resolved SAXS investigations of the Lee–Meisel synthesis. Scattering curves for (a) large q and (b) small q values. The results shown were obtained from two separated experiments.

remains unclear. The first evaluable scattering intensity was detected at about 30 min. The scattering corresponds to relatively large particles. Assuming a spherical particle shape, the mean radius is ~ 13 nm at a polydispersity of $\sim 30\%$ (see Supporting Information SI-7). In the course of the reaction, the scattering intensity increases only in the low q range which corresponds either to the growth of the already existing particles or the formation of further large particles. The relative number of particles and volume fraction cannot be determined from the SAXS curves because the AgNP at all reaction times are too large, polydisperse and most likely also nonuniformly shaped. It is also not possible to determine the point of full precursor reduction. Although the growth mechanism of the Lee–Meisel synthesis cannot be deduced from these experiments, it is clearly not similar to the Turkevich seed-mediated growth mechanism. The processes which create the fortunate coincident in the first seconds of the Turkevich reaction do not appear for the Lee–Meisel synthesis. This might be due to the fact that, although the silver ion could exist in different species (e.g., different aqua complexes), no chemical process which transforms a reactive into a less reactive silver precursor species is available which triggers the formation of seed particles. As a result, the final AgNPs are nonuniformly shaped, polydisperse and large (size range of 30 nm in radius).

Summary #5. The growth mechanism of the reduction of AgNO_3 with Na_3Ct (known as Lee–Meisel synthesis) is not similar to the Turkevich synthesis. The chemical processes occurring during the Lee–Meisel synthesis does not ensure a certain phase in which a defined amount of Ag monomers for the formation of seed particles is delivered. Therefore, the synthesis leads to relatively large particles at high polydispersities and is not reproducible with respect to size, polydispersity and morphology.

CONCLUSIONS

This contribution provides a comprehensive picture of the Turkevich synthesis which includes the relevant underlying physicochemical processes. The gained

knowledge enables more than a growth characterization by a detailed growth mechanism. It allows understanding what determines the final particle size and illustrating the influence of reaction conditions on the growth process and thus the final size.

In question #1 it is shown that the previously described³² four-step growth mechanism is valid for a wide range of reaction conditions. The first step is a partial reduction of the gold precursor and the formation of small clusters from the Au monomers. In a second step, these clusters form seed particles with radii > 1.5 nm. The third and fourth steps comprise the reduction of the residual ionic gold (first slowly, then fast) whereby the generated gold monomers grow exclusively on top of the seeds until the precursor is fully consumed. Therefore, no further particles are formed during the last two steps. The described 4-step growth mechanism can be referred as seed-mediated growth mechanism.

The mechanism leads to monodisperse AuNP since only a slight amount of the ionic gold is reduced during the seed particle formation (see question #2). The few formed seed particles are polydisperse^{26,53} but grow into monodisperse AuNP due to a continuous monomer supply during growth steps 3 and 4 which could be described by a size focusing effect.⁵⁴

The seed-mediated growth mechanism is actually a fortunate coincidence created by a favorable interplay of different chemical and physicochemical processes as shown in question #3 and illustrated in Figure 8. The first important aspect of the fortunate coincidence is the initiation of seed particle formation in the initial phase of the synthesis. Au monomers are supplied by the fast reduction of reactive $[\text{AuCl}_4]^-$. Moreover, the standard reaction conditions are moderate enough to allow the formation of colloidally stable small seed particles from these monomers. The second aspect of the fortunate coincidence is the termination of seed particle formation just within an appropriate time frame so that only “very few” seed particles (still in the scale of trillions) are formed. This aspect is a result of

the buffer effect of Na_3Ct and the pH-dependent ligand exchange equilibrium of gold complexes. Upon mixing the reactants, Na_3Ct increases the pH level of the gold precursor solution inducing the transformation of the reactive $[\text{AuCl}_4]^-$ into less reactive $[\text{AuCl}_{3-x}(\text{OH})_{1+x}]^-$ species. This transformation quenches the fast monomer supply in solution and constitutes the end of step 2 of the growth mechanism. The third aspect of the fortunate coincidence is the exclusive growth of residual gold onto the seed particles during growth steps 3 and 4. The reduction of $[\text{AuCl}_{3-x}(\text{OH})_{1+x}]^-$ species at the surface of the particles is favored over the reduction "in solution". DCA is formed as chemical product of the reduction of Au^{3+} by citrate. It accelerates the reduction process but has no effect on the final particle size in the standard Turkevich synthesis.

The understanding of the origin of the seed-mediated growth mechanism reveals how the final particle size is determined. The final size is already determined at a very early stage of the synthesis—after the end of seed particle formation (after step 2 of the growth mechanism). Since no further particles are formed during growth steps 3 and 4, the final total number of AuNP is equivalent to the number of seed particles and determines to how many particles the total amount of Au (depends on initial HAuCl_4 concentration) is distributed. The number of seed particles is determined by two factors as illustrated in Figure 4 in question #3: (i) the amount of Au monomers which is available during the seed particle formation; if more monomers are available, more seed particles can be formed and the total amount of gold is distributed to more particles leading to a smaller final size; and (ii)

the minimum size of the seed particles determined by the colloidal stability; if seed particles are stable at larger sizes, less particles can be formed from the available monomers leading to larger final AuNP. These factors are determined by the reaction conditions since they influence either the reduction chemistry during seed particle formation, the colloidal stability of the seed particles or both.

Taking these two pathways into consideration, it is possible to understand and illustrate the influences of reaction conditions on the final NP size. In question #4, the influences of parameters such as concentration, pH value, order of reactant addition and synthesis temperature are discussed in detail. Furthermore, the boundaries of the seed-mediated growth mechanism are identified. For extreme reaction conditions (strong deviation from standard synthesis protocol), the fortunate coincidence vanishes as soon as one of its conditions is no longer fulfilled. This leads to the synthesis of polydisperse and large particles up to gold precipitates.

Any seed-mediated growth mechanism demands an interplay of processes that start and terminate a seed particle formation step. For the citrate reduction of AgNO_3 , known as Lee-Meisel synthesis, the absence of conditions which create a seed-mediated growth mechanism results in large and polydisperse AgNP (see #5).

In principle, the picture of parameter influences on the final particle size presented for the Turkevich synthesis might be representative for other colloidal syntheses which comprise a seed-mediated growth mechanism.

EXPERIMENTAL SECTION

Colloidal Syntheses. Chemicals. HAuCl_4 (99.999%), AgNO_3 (99.9999%), $\text{Na}_3\text{Ct} \cdot 2\text{H}_2\text{O}$ ($\geq 99\%$), $\text{NaClO}_4 \cdot 2\text{H}_2\text{O}$ (98%) and 1,3-dicarboxyacetone (technical grade) were purchased from Sigma-Aldrich. All solution were prepared using Milli-Q water. The labware was cleaned after each synthesis using *aqua regia* and Milli-Q water.

Standard Turkevich Synthesis. A volume of 199 mL of a 0.25 mM HAuCl_4 solution was refluxed in a round-bottomed flask equipped with a condenser for 15 min. One milliliter of a freshly prepared 500 mM Na_3Ct solution was added quickly (final concentration $[\text{Na}_3\text{Ct}] = 2.5$ mM). The mixture was refluxed until the precursor was completely reduced. The overall reaction time can be determined by observing the solution until a characteristic ruby red color is obtained.

Lee-Meisel Synthesis. One liter of a 0.5 mM AgNO_3 solution (freshly prepared) and one liter of a 0.5 mM Na_3Ct solution were heated to 85 °C. The reducing agent was added quickly to the metal precursor (final concentrations $[\text{AgNO}_3] = 0.25$ mM, $[\text{Na}_3\text{Ct}] = 2.5$ mM). The obtained mixture was kept at 85 °C.

Comments on Parameter Variation Studies. The standard protocol was maintained in all points which were not addressed by a certain parameter variation. For the variation of ionic strength, NaClO_4 was added in different amounts to the Na_3Ct solution prior to mixing with HAuCl_4 . For the pH variation, the initial pH of the HAuCl_4 solution was varied by addition of HCl or NaOH. Note that the kinetics of the complex equilibrium is at

room temperature in the range of several minutes. Therefore, the pH value of the HAuCl_4 solution cannot be determined directly after addition of HCl or NaOH. For the inverse method, 199 mL of a 2.5 mM Na_3Ct solution was refluxed and 1 mL of a 50 mM HAuCl_4 solution was added.

Ex Situ Characterization. For SEM imaging, a sample droplet was deposited on a Si/TiO_2 wafer and removed immediately with an Eppendorf pipet. Measurements were performed on a JEOL JSM-7401F (Hitachi Ltd., Tokyo, Japan) with an acceleration voltage of 10 kV at a working distance of 8 mm. For TEM imaging, a sample droplet was deposited on a copper grid and removed immediately with an Eppendorf pipet. Measurements were performed on a FEI Tecnai G2 20 S-TWIN instrument operated at 200 kV (images displayed in Figure 2 and Supporting Information SI-3) and on a Philips CM200 LaB₆ operated at an acceleration voltage of 200 kV, respectively (images displayed in Supporting Information SI-2).

UV–Vis Spectroscopy. UV–vis spectra were recorded on an Evolution 220 (Thermo Fischer Scientific). For time-resolved measurements, an external cuvette holder with heating and temperature control function was connected to the spectrometer via fiber optical cables. Measurements were carried out in a quartz cuvette.

Small Angle X-ray Scattering (SAXS) and Ultrasmall Angle X-ray Scattering (USAXS) Experiments. Synchrotron SAXS Investigations. The synchrotron SAXS investigations were performed at the ID02 beamline (ESRF) using a free-liquid jet setup. Details are

describe elsewhere.²⁷ The distance between reaction vessel and jet was minimized to achieve a low dead time (approximately 5 s) and to avoid agglomeration of the particles inside the tubings. The technique offers the possibility to follow the nanoparticle growth *in situ* with a time-resolution that is limited just by the photon flux and the acquisition time of the detector. In addition, X-ray induced effects are minimized, and contamination problems (contamination of capillary walls) are eliminated.

Synchrotron SAXS Investigations. SAXS measurements were performed at the B1 beamline (DORIS III) using a flow-through capillary.

Lab-Scale SAXS Investigations of Final Colloidal Solutions. The scattering curves of the final colloidal solutions were recorded on a SAXS instrument (SAXSess, Anton Paar GmbH) using a quartz flow cell.

SAXS Evaluation. The scattering curves of the colloidal solution were analyzed assuming spherical shape, a homogeneous electron density, and a Schulz-Zimm size distribution. The Schulz-Zimm distribution is given by

$$f(r) = (z+1)^{z+1} x^z \frac{\exp[-(z+1)x]}{R_{\text{avg}} \Gamma(z+1)} \quad (1)$$

where R_{avg} is the mean radius, $x = r/R_{\text{avg}}$, z is related to the polydispersity p ($p = \sigma/R_{\text{avg}}$) by $z = 1/p^2 - 1$, and σ^2 is the variance of the distribution. The scattering intensity of nonaggregated particles can be assumed to be proportional to the form factor of a single particle $P(q)$. Thus, the scattering intensity of N monodisperse spheres with homogeneous electron density and volume V_{part} is given by

$$\begin{aligned} I(q) &= NI_{\text{part}}(q) = NV_{\text{part}}^2 P(q) \\ &= NV_{\text{part}}^2 \left[\Delta\rho \frac{3(\sin(qR) - qR\cos(qR))}{qR} \right]^2 \end{aligned} \quad (2)$$

In case of polydisperse spherical particles, one has to sum the scattering intensities over all particle sizes weighted by their frequency as given by the size distribution function. It is common to use the Schulz-Zimm distribution for polydisperse particles. Hence, the scattering intensity is given by

$$I(q) = N \int_0^\infty f(r) V_{\text{part}}^2 P(q) dr \quad (3)$$

An analytical solution of the integral can be found in Kotlarchyk *et al.*⁵⁵ To analyze the growth mechanism of nanoparticles, the number of particles is important. This information can be obtained by using the general relation of $I(q=0) = (\Delta\rho)^2 V_{\text{part}}^2$ for a single particle. Thus, the scattered intensity $I(q=0)$ of polydisperse particles can be written as

$$I(q=0) = N \langle V^2 \rangle (\Delta\rho)^2 \quad (4)$$

where N is the number of particles and $\langle V^2 \rangle$ is the mean value of V_{part}^2 . Due to the overlapping of the scattering intensity with the primary beam, $I(q=0)$ cannot be measured directly, but is accessible *via* the extrapolation of $I(q)$ for $q \rightarrow 0$. Selected scattering curves and mathematical fits can be found in Supporting Information SI-7.

The equation to calculate the relative number of particles in Table 1 is derived from the average volume:

$$\langle V \rangle = \frac{4\pi}{3} \langle R^3 \rangle = \frac{4\pi}{3} \langle R_{\text{avg}} \rangle^3 \frac{(z+3)(z+2)}{(z+1)^2} \quad (5)$$

Since the polydispersities of the colloidal solutions investigated in Table 1 are the same (10%), it follows that $\langle V_1 \rangle / \langle V_2 \rangle = \langle R_{\text{avg},1} \rangle^3 / \langle R_{\text{avg},2} \rangle^3$.

Conflict of Interest: The authors declare no competing financial interest.

Supporting Information Available: Scheme of the general growth mechanisms, SAXS, SEM, TEM, UV-vis data of AuNP syntheses and precursor investigations. The Supporting Information is available free of charge on the ACS Publications website at DOI: 10.1021/acsnano.5b01579.

Acknowledgment. J.P. acknowledges generous funding by the Deutsche Forschungsgemeinschaft within the project PO 1744/1-1. M.W. acknowledges financial support by the Fonds der Chemischen Industrie. R.K. thanks in particular Einstein Foundation Berlin for generous support provided by an Einstein-Junior-Fellowship (EJF-2011-95). R.K. also acknowledges funding from BMBF (FKZ 03EK3009). The authors acknowledge the European Synchrotron Radiation Facility for provision of synchrotron radiation facilities and would like to thank Dr. T. Narayanan for assistance in using beamline ID02 for SAXS measurements. SAXS measurements were conducted at beamline B1 at light source DORIS III at DESY, a member of the Helmholtz Association (HGF).

REFERENCES AND NOTES

- Zhao, P.; Li, N.; Astruc, D. State of the Art in Gold Nanoparticle Synthesis. *Coord. Chem. Rev.* **2013**, *257*, 638–665.
- Ojea-Jiménez, I.; Romero, F. M.; Bastús, N. G.; Puntes, V. Small Gold Nanoparticles Synthesized with Sodium Citrate and Heavy Water: Insights into the Reaction Mechanism. *J. Phys. Chem. C* **2010**, *114*, 1800–1804.
- Ojea-Jiménez, I.; Bastús, N. G.; Puntes, V. Influence of the Sequence of the Reagents Addition in the Citrate-Mediated Synthesis of Gold Nanoparticles. *J. Phys. Chem. C* **2011**, *115*, 15752–15757.
- Doyen, M.; Bartik, K.; Brulyants, G. UV–Vis and NMR Study of the Formation of Gold Nanoparticles by Citrate Reduction: Observation of Gold–citrate Aggregates. *J. Colloid Interface Sci.* **2013**, *399*, 1–5.
- Kimling, J.; Maier, M.; Okenve, B.; Kotaidis, V.; Ballot, H.; Plech, A. Turkevich Method for Gold Nanoparticle Synthesis Revisited. *J. Phys. Chem. B* **2006**, *110*, 15700–15707.
- Turkevich, J.; Stevenson, P. C.; Hillier, J. A Study of the Nucleation and Growth Processes in the Synthesis of Colloidal Gold. *Discuss. Faraday Soc.* **1951**, *11*, 55–75.
- Hauser, E. A.; Lynn, J. E. *Experiments in Colloid Chemistry*; McGraw-Hill: New York, 1940.
- Frens, G. Controlled Nucleation for Regulation of Particle-Size in Monodisperse Gold Suspensions. *Nature, Phys. Sci.* **1973**, *241*, 20–22.
- Chow, M. K.; Zukoski, C. F. Gold Sol Formation Mechanisms: Role of Colloidal Stability. *J. Colloid Interface Sci.* **1994**, *165*, 97–109.
- Freund, P. L.; Spiro, M. Colloidal Catalysis: The Effect of Sol Size and Concentration. *J. Phys. Chem.* **1985**, *89*, 1074–1077.
- Engelbrekt, C.; Jensen, P. S.; Sørensen, K. H.; Ulstrup, J.; Zhang, J. Complexity of Gold Nanoparticle Formation Disclosed by Dynamics Study. *J. Phys. Chem. C* **2013**, *117*, 11818–11828.
- Turkevich, J.; Stevenson, P. C.; Hillier, J. The Formation of Colloidal Gold. *J. Phys. Chem.* **1953**, *57*, 670–673.
- LaMer, V. K.; Kenyon, A. S. Kinetics of the Formation of Monodispersed Sulfur Solns from Thiosulfate and Acid. *J. Colloid Sci.* **1947**, *2*, 257–264.
- Takiyama, K. Formation and Aging of Precipitates. VIII. Formation of Monodisperse Particles (1) Gold Sol Particles by Sodium Citrate Method. *Bull. Chem. Soc. Jpn.* **1958**, *31*, 944–950.
- Hendel, T.; Wuithschick, M.; Kettemann, F.; Birnbaum, A.; Rademann, K.; Polte, J. In Situ Determination of Colloidal Gold Concentrations with UV–Vis Spectroscopy: Limitations and Perspectives. *Anal. Chem.* **2014**, *86*, 11115–11124.
- Pei, L.; Mori, K.; Adachi, M. Formation Process of Two-Dimensional Networked Gold Nanowires by Citrate Reduction of AuCl4- and the Shape Stabilization. *Langmuir* **2004**, *20*, 7837–7843.
- Rodríguez-González, B.; Mulvaney, P.; Liz-Marzán, L. M. An Electrochemical Model for Gold Colloid Formation via Citrate Reduction. *Z. Phys. Chem.* **2007**, *221*, 415–426.
- Pong, B.-K.; Elim, H. I.; Chong, J.-X.; Ji, W.; Trout, B. L.; Lee, J.-Y. New Insights on the Nanoparticle Growth Mechanism in the Citrate Reduction of Gold(III) Salt: Formation of the

- Au Nanowire Intermediate and Its Nonlinear Optical Properties. *J. Phys. Chem. C* **2007**, *111*, 6281–6287.
19. Ji, X.; Song, X.; Li, J.; Bai, Y.; Yang, W.; Peng, X. Size Control of Gold Nanocrystals in Citrate Reduction: The Third Role of Citrate. *J. Am. Chem. Soc.* **2007**, *129*, 13939–13948.
 20. Mikhlin, Y.; Karacharov, A.; Likhatski, M.; Podlipskaya, T.; Zubavichus, Y.; Veligzhanin, A.; Zaikovski, V. Submicrometer Intermediates in the Citrate Synthesis of Gold Nanoparticles: New Insights into the Nucleation and Crystal Growth Mechanisms. *J. Colloid Interface Sci.* **2011**, *362*, 330–336.
 21. Zhao, L.; Jiang, D.; Cai, Y.; Ji, X.; Xie, R.; Yang, W. Tuning the Size of Gold Nanoparticles in the Citrate Reduction by Chloride Ions. *Nanoscale* **2012**, *4*, 5071–5076.
 22. Patungwasa, W.; Hodak, J. H. pH Tunable Morphology of the Gold Nanoparticles Produced by Citrate Reduction. *Mater. Chem. Phys.* **2008**, *108*, 45–54.
 23. Kumar, S.; Gandhi, K. S.; Kumar, R. Modeling of Formation of Gold Nanoparticles by Citrate Method. *Ind. Eng. Chem. Res.* **2007**, *46*, 3128–3136.
 24. Finney, E. E.; Finke, R. G. Nanocluster Nucleation and Growth Kinetic and Mechanistic Studies: A Review Emphasizing Transition-Metal Nanoclusters. *J. Colloid Interface Sci.* **2008**, *317*, 351–374.
 25. Georgiev, P.; Bojinova, A.; Kostova, B.; Momekova, D.; Bjornholm, T.; Balashev, K. Implementing Atomic Force Microscopy (AFM) for Studying Kinetics of Gold Nanoparticle's Growth. *Colloids Surf., A* **2013**, *434*, 154–163.
 26. Polte, J.; Ahner, T. T.; Delissen, F.; Sokolov, S.; Emmerling, F.; Thünemann, A. F.; Krahnert, R. Mechanism of Gold Nanoparticle Formation in the Classical Citrate Synthesis Method Derived from Coupled In Situ XANES and SAXS Evaluation. *J. Am. Chem. Soc.* **2010**, *132*, 1296–1301.
 27. Polte, J.; Erler, R.; Thünemann, A. F.; Emmerling, F.; Krahnert, R. SAXS in Combination with a Free Liquid Jet for Improved Time-Resolved In Situ Studies of the Nucleation and Growth of Nanoparticles. *Chem. Commun.* **2010**, *46*, 9209–9211.
 28. Ojea-Jiménez, I.; Campanera, J. M. Molecular Modeling of the Reduction Mechanism in the Citrate-Mediated Synthesis of Gold Nanoparticles. *J. Phys. Chem. C* **2012**, *116*, 23682–23691.
 29. Abecassis, B.; Testard, F.; Kong, Q.; Francois, B.; Spalla, O. Influence of Monomer Feeding on a Fast Cold Nanoparticles Synthesis: Time-Resolved XANES and SAXS Experiments. *Langmuir* **2010**, *26*, 13847–13854.
 30. Polte, J.; Tuaev, X.; Wuithschick, M.; Fischer, A.; Thünemann, A. F.; Rademann, K.; Krahnert, R.; Emmerling, F. Formation Mechanism of Colloidal Silver Nanoparticles: Analogies and Differences to the Growth of Gold Nanoparticles. *ACS Nano* **2012**, *6*, 5791–5802.
 31. Wuithschick, M.; Paul, B.; Bienert, R.; Sarfraz, A.; Vainio, U.; Sztucki, M.; Krahnert, R.; Strasser, P.; Rademann, K.; Emmerling, F.; et al. Size-Controlled Synthesis of Colloidal Silver Nanoparticles Based on Mechanistic Understanding. *Chem. Mater.* **2013**, *25*, 4679–4689.
 32. Polte, J. Fundamental Growth Principles of Colloidal Metal Nanoparticles - a new Perspective. *CrystEngComm* **2015**, DOI: 10.1039/C5CE01014D.
 33. Daniel, M.-C.; Astruc, D. Gold Nanoparticles: Assembly, Supramolecular Chemistry, Quantum-Size-Related Properties, and Applications toward Biology, Catalysis, and Nanotechnology. *Chem. Rev.* **2004**, *104*, 293–346.
 34. Verwey, J. T. G. Theory of the Stability of Lyophobic Colloids. *J. Phys. Colloid Chem.* **1947**, *51*, 631–636.
 35. Derjaguin, B.; Landau, L. Theory of Stability of Highly Charged Liophobic Sols and Adhesion of Highly Charged Particles in Solutions of Electrolytes. *Zh. Eksp. Teor. Fiz.* **1945**, *15*, 663–682.
 36. Wuithschick, M.; Witte, S.; Kettemann, F.; Rademann, K.; Polte, J. Illustrating the Formation of Metal Nanoparticles with a Growth Concept Based on Colloidal Stability. *Phys. Chem. Chem. Phys.* **2015**, DOI: 10.1039/C5CP02219C.
 37. Zabetakis, K.; Ghann, W. E.; Kumar, S.; Daniel, M.-C. Effect of High Gold Salt Concentrations on the Size and Polydispersity of Gold Nanoparticles Prepared by an Extended Turkevich-Frens Method. *Gold Bull.* **2012**, *45*, 203–211.
 38. Wang, S.; Qian, K.; Bi, X. Z.; Huang, W. Influence of Speciation of Aqueous HAuCl₄ on the Synthesis, Structure, and Property of Au Colloids. *J. Phys. Chem. C* **2009**, *113*, 6505–6510.
 39. Murphy, P. J.; LaGrange, M. S. Raman Spectroscopy of Gold Chloro-Hydroxy Speciation in Fluids at Ambient Temperature and Pressure: A Re-Evaluation of the Effects of pH and Chloride Concentration. *Geochim. Cosmochim. Acta* **1998**, *62*, 3515–3526.
 40. Peck, J. A.; Tait, C. D.; Swanson, B. I.; Brown, G. E., Jr. Speciation of Aqueous gold(III) Chlorides from Ultraviolet/visible Absorption and Raman/resonance Raman Spectroscopies. *Geochim. Cosmochim. Acta* **1991**, *55*, 671–676.
 41. Goia, D. V.; Matijević, E. Tailoring the Particle Size of Monodispersed Colloidal Gold. *Colloids Surf., A* **1999**, *146*, 139–152.
 42. Shiba, F. Size Control of Monodisperse Au Nanoparticles Synthesized via a Citrate Reduction Process Associated with a pH-Shifting Procedure. *CrystEngComm* **2013**, *15*, 8412–8415.
 43. Xia, H.; Bai, S.; Hartmann, J.; Wang, D. Synthesis of Monodisperse Quasi-Spherical Gold Nanoparticles in Water via Silver(I)-Assisted Citrate Reduction. *Langmuir* **2010**, *26*, 3585–3589.
 44. Kuyper, A. C. The Oxidation of Citric Acid. *J. Am. Chem. Soc.* **1933**, *55*, 1722–1727.
 45. Barbooti, M. M.; Al-Sammerrai, D. A. Thermal Decomposition of Citric Acid. *Thermochim. Acta* **1986**, *98*, 119–126.
 46. Sivaraman, S. K.; Kumar, S.; Santhanam, V. Monodisperse Sub-10 nm Gold Nanoparticles by Reversing the Order of Addition in Turkevich Method - The Role of Chloroauric Acid. *J. Colloid Interface Sci.* **2011**, *361*, 543–547.
 47. Li, C.; Li, D.; Wan, G.; Xu, J.; Hou, W. Facile Synthesis of Concentrated Gold Nanoparticles with Low Size-Distribution in Water: Temperature and pH Controls. *Nanoscale Res. Lett.* **2011**, *6*, 440.
 48. Lee, P. C.; Meisel, D. Adsorption and Surface-Enhanced Raman of Dyes on Silver and Gold Sols. *J. Phys. Chem.* **1982**, *86*, 3391–3395.
 49. Pillai, Z. S.; Kamat, P. V. What Factors Control the Size and Shape of Silver Nanoparticles in the Citrate Ion Reduction Method? *J. Phys. Chem. B* **2004**, *108*, 945–951.
 50. Dong, X.; Ji, X.; Wu, H.; Zhao, L.; Li, J.; Yang, W. Shape Control of Silver Nanoparticles by Stepwise Citrate Reduction. *J. Phys. Chem. C* **2009**, *113*, 6573–6576.
 51. Gorup, L. F.; Longo, E.; Leite, E. R.; Camargo, E. R. Moderating Effect of Ammonia on Particle Growth and Stability of Quasi-Monodisperse Silver Nanoparticles Synthesized by the Turkevich Method. *J. Colloid Interface Sci.* **2011**, *360*, 355–358.
 52. Šileikaitė, A.; Prosyčėvas, I.; Puišo, J.; Juraitis, A.; Guobienė, A. Analysis of Silver Nanoparticles Produced by Chemical Reduction of Silver Salt Solution. *Mater. Sci.* **2006**, *12*, 287–291.
 53. Polte, J.; Herder, M.; Erler, R.; Rolf, S.; Fischer, A.; Würth, C.; Thünemann, A. F.; Krahnert, R.; Emmerling, F. Mechanistic Insights into Seeded Growth Processes of Gold Nanoparticles. *Nanoscale* **2010**, *2*, 2463–2469.
 54. Reiss, H. The Statistical Mechanical Theory of Irreversible Condensation. *J. Chem. Phys.* **1952**, *20*, 1216–1227.
 55. Kotlarchyk, M.; Chen, S.-H. Analysis of Small Angle Neutron Scattering Spectra from Polydisperse Interacting Colloids. *J. Chem. Phys.* **1983**, *79*, 2461–2469.